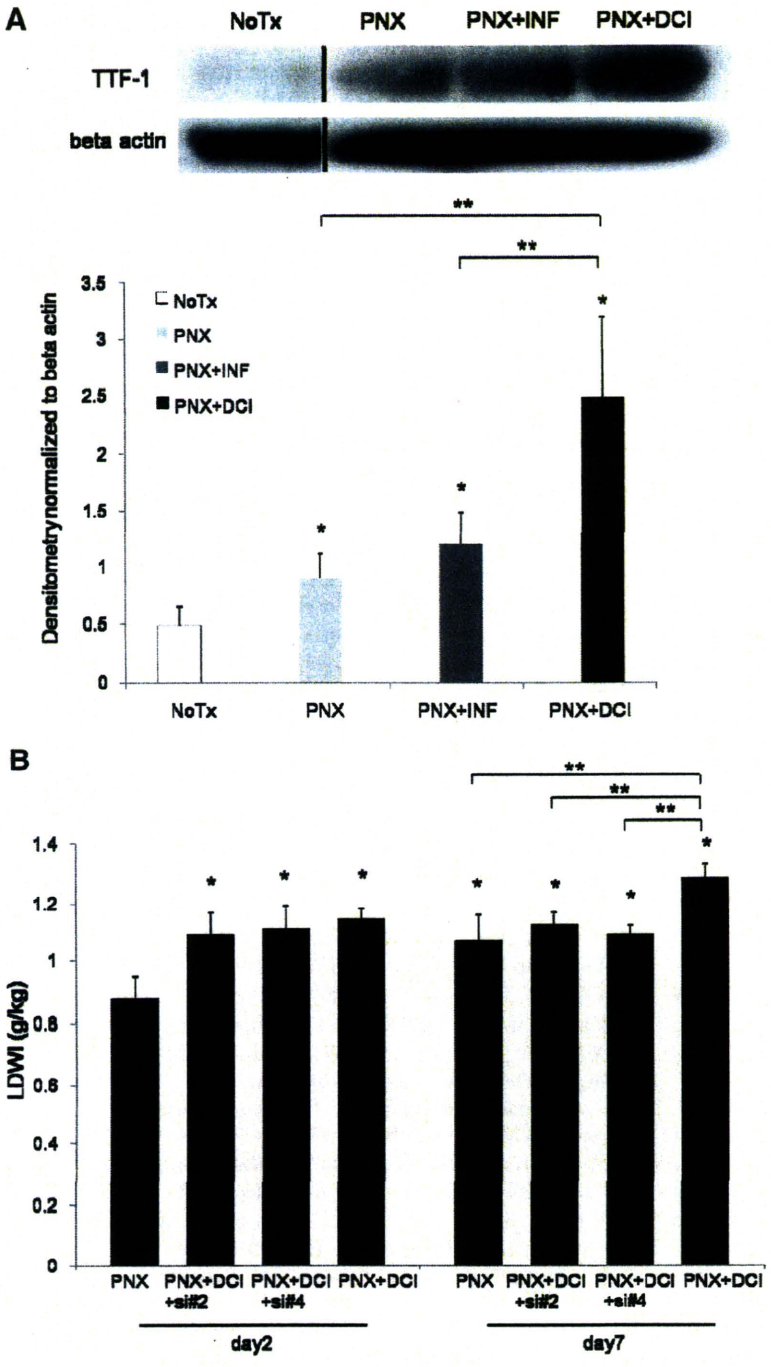

Fig. 2. *A*: Western blot analysis showed that thyroid transcription factor 1 (TTF-1) expression in the residual right lung at *day 2* was significantly increased in the PNX+DCI group compared with PNX only (PNX group), PNX+INF group, or the NoTx group. The NoTx group and the respective β-actin is from a different gel. Band densitometry was quantified using Image J. Values were normalized to β-actin. $*P < 0.05$ vs. NoTx group, $**P < 0.05$ between the indicated groups. *B*: increase in right LDWI by DCI administration after left pneumonectomy was not affected by coadministration of TTF-1 inhibitory RNAs (TTF-1 siRNAs), si#2, and si#4, at *day 2* ($n = 5$ in each group) but was significantly suppressed at *day 7* by both sequences of TTF-1 siRNAs ($n = 5$ in each group). $*P < 0.05$ vs. NoTx group, $**P < 0.05$ between the indicated groups.

DISCUSSION

In the present study, compensatory lung growth was modestly but significantly facilitated by airway administration of DCI, as indicated by the increase in LDW and LDWI. Morphological analyses suggested that DCI administration increased the number alveoli, made each of them smaller, and produced a net increase in the total alveolar area per field and the calculated surface area of the alveoli per volume of lung. Similar findings have been reported with retinoic acid (4, 21, 22) and estrogen (19, 20). These findings may merely represent an imbalance between septation and septal cell proliferation, but it is also possible that DCI administration reduced lung elasticity. To this end, at least morphologically, there were no apparent indications of atelectasis, pleural thickening, septal thickening, or inflammation in the PNX+DCI group. There was also no significant difference between the PNX+INF group and the PNX+DCI group in transpulmonary pressure at *day 14*. Therefore, the spatial constraint due to the predetermined volume of the chest cavity, which presumably resulted in the lack of significant increase in LVI, may

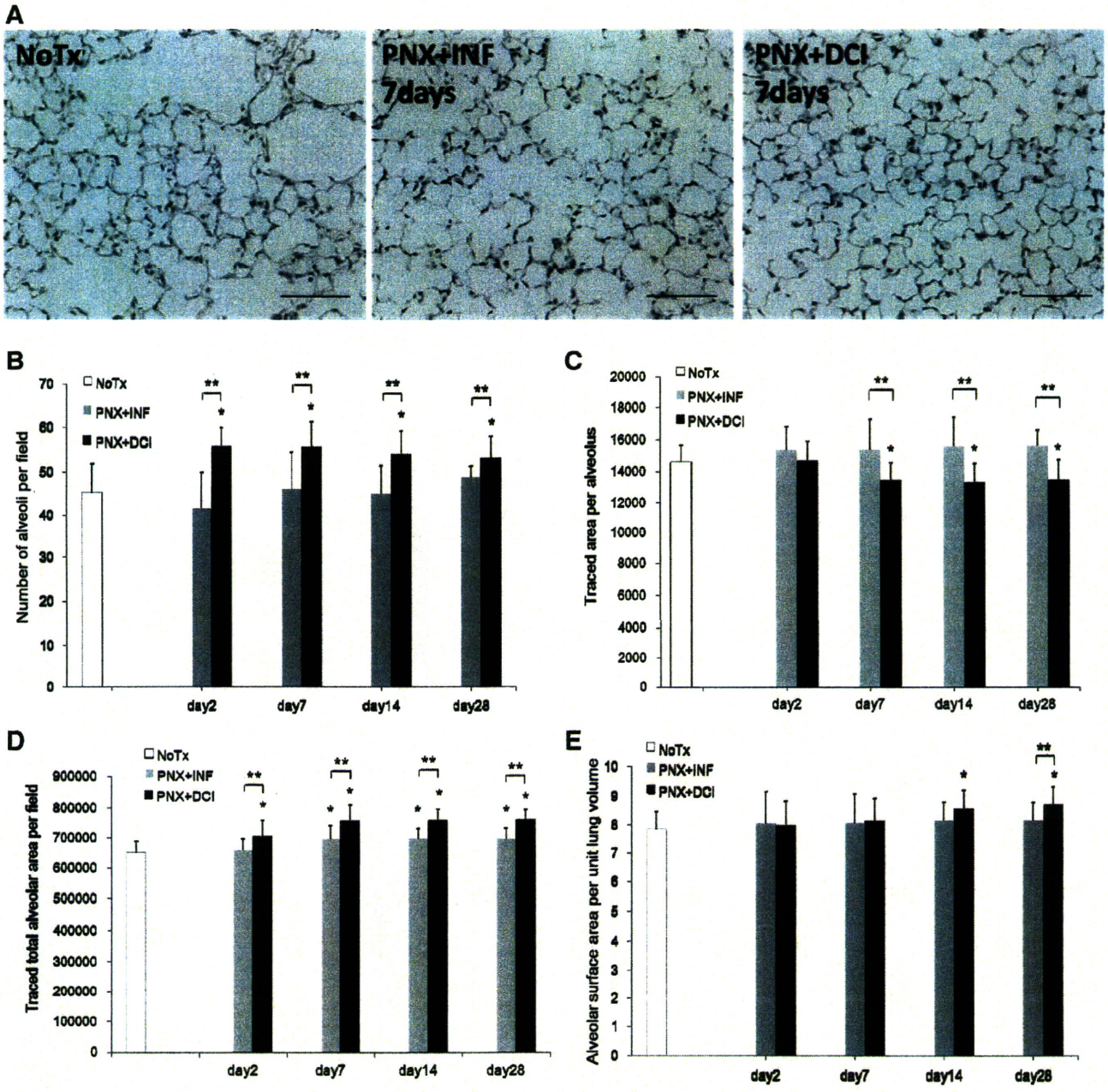

Fig. 3. Morphological findings. *A*: on morphology at *day 7*, the alveoli appeared to be smaller in the PNX+DCI group compared with the PNX+INF group or the NoTx group. Hematoxylin-and-eosin staining, scale bar 100 μm. *B*: on morphological analysis, the number of alveoli per field of view was significantly increased in the PNX+DCI (n = 5, 25 fields for each time point) group compared with the PNX+INF (n = 5; 25 fields for each time point) group and the NoTx (n = 5; 25 fields for each time point) group throughout the experiment. *C*: average traced area of a single alveolus on morphology was significantly decreased in the PNX+DCI (n = 5; 25 fields for each time point) group compared with the PNX+INF (n = 5; 25 fields for each time point) group, and the NoTx (n = 5; 25 fields for each time point) group beyond 7 days. *D*: average total alveolar area per field on morphology was significantly increased in the PNX+DCI (n = 5; 25 fields for each time point) group compared with the PNX+INF (n = 5; 25 fields for each time point) group and the NoTx (n = 5; 25 fields for each time point) group beyond 2 days. *E*: calculated surface area of the alveoli per volume of lung was significantly increased in the PNX+DCI (n = 5; 25 fields for each time point) group compared with the PNX+INF (n = 5; 25 fields for each time point) group and the NoTx (n = 5; 25 fields for each time point) group beyond *day 14*. *$P < 0.05$ vs. NoTx group, **$P < 0.05$ between the indicated groups.

at least, in part, be the reason for these findings. Since morphological analyses were carried out in fixed specimens, it is also not possible to completely rule out the possibility that the fixation-induced shrinkage may have been different among groups. Further studies looking into the extracellular matrix components may resolve some of these issues, but collectively, the data suggest that the increase in LDWI was primarily due to the increase in the number of alveoli. If so, increased number of small alveoli may have actually augmented lung function within a fixed lung volume (19). To

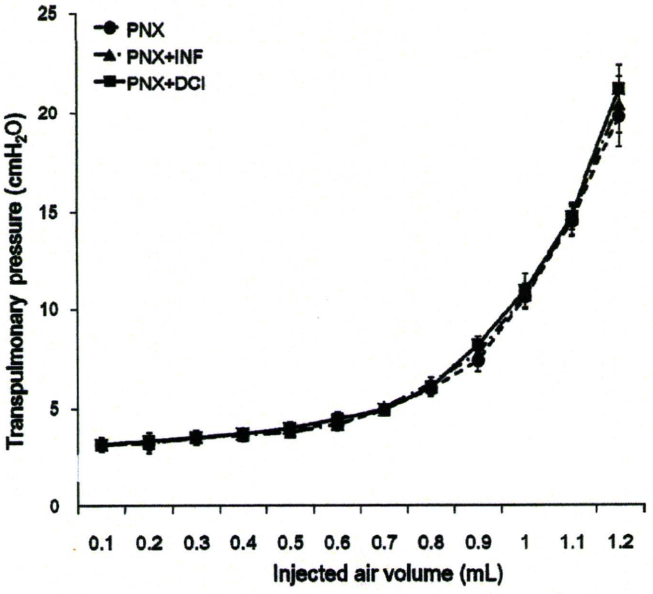

Fig. 4. Transpulmonary pressure measurements were made using a water manometer at increments of 0.1 ml. The curve shape was not significantly different between the PNX group (n = 5), PNX+INF group (n = 5) and the PNX+DCI group (n = 5).

this end, exercise capability, particularly forced exercise, which has been reported to reflect lung function (23), was better sustained in the PNX+DCI group compared with the PNX+INF group, although it is possible that factors other than lung function may also have contributed to this difference. The results of the semivoluntary wheel-running test, at least in part, rules out the possibility that DCI administration caused alterations in spontaneous activity of mice, which may have influenced the results of the exercise tests. To this end, more detailed specific lung function tests are required.

Glucocorticoids potentially induce developmental lung growth (1) but is reported to have no apparent effect on compensatory lung growth by systemic administration (25). Induction of cAMP has been shown to facilitate fetal lung maturation (2), and in combination with dexamethasone, this facilitation has been shown to be synergistic (8). The exact mechanism of this synergy remains unclear, and furthermore, the effects of glucocorticoids on developmental and postnatal lung growth seem to be context dependent. Developmental, postnatal, and postpneumonectomy compensatory lung growth may be regulated through different pathways although not mutually exclusive. Hence, it is possible that glucocorticoids and cAMP, individually and in combination, may act differently on each of the lung growth processes. Caution in the use of dexamethasone may be required since prolonged systemic administration of glucocorticoids, particularly at high doses, are reported to be detrimental to postnatal lung growth (6, 26). Although the combined effects of the components of DCI may be substantially different from the effects of glucocorticoids alone, it is nevertheless encouraging that in the present study, the effect of a single administration of DCI was sustained for at least 28 days. Although we have not done any pharmacokinetic studies, it is unlikely that the effect of DCI per se was sustained throughout this period, suggesting that facilitation of initial stimuli for compensatory lung growth is important rather than its maintenance. Therefore, prolonged administration may not be necessary. Furthermore, administration of DCI without pneumonectomy did not demonstrate any overt effects (data not shown), suggesting that DCI only augments compensatory lung growth. To this end, the optimal timing of DCI administration in relation to pneumonectomy, along with the potential duration of action of DCI is considered to be important and requires further study.

In the present study, we used INF as a vehicle since it is in clinical use as a surfactant supplement and is experimentally

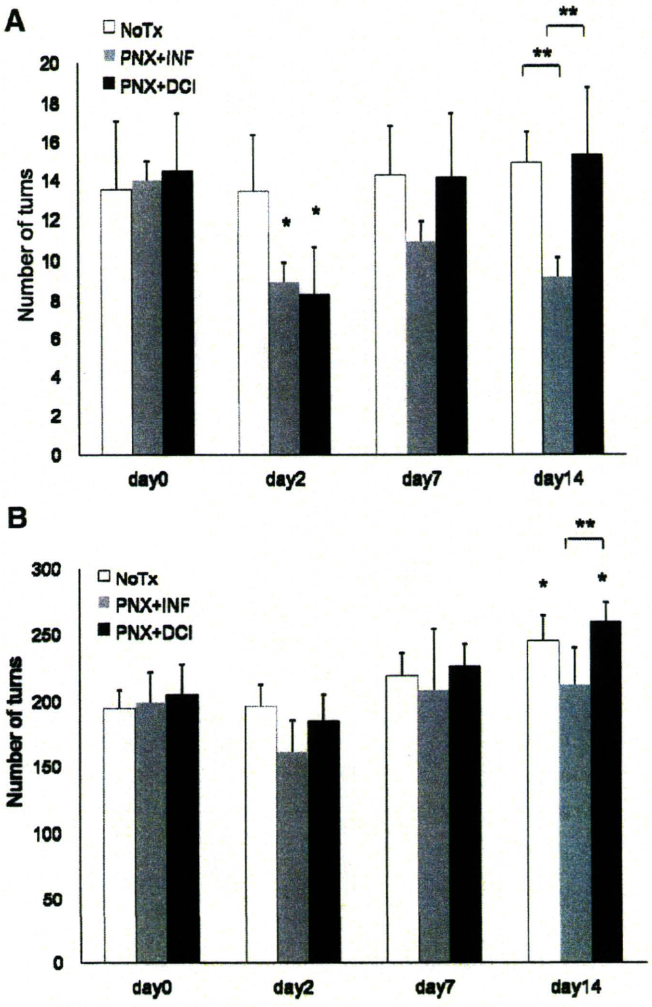

Fig. 5. Exercise tests as indirect indices of lung function. *A*: forced wheel running at *day 0*, prior to pneumonectomy, did not differ significantly between groups (n = 4 in each group). Forced wheel running at *day 2* was significantly reduced in both PNX+DCI and PNX+INF groups compared with the respective values at *day 0*. Recovery was seen beyond *day 7* in the PNX+DCI group but not in the PNX+INF group. $*P < 0.05$ vs. respective *day 0* values, $**P < 0.05$ between the indicated groups. *B*: semivoluntary wheel running at *day 2* (n = 4 in each group) tended to be reduced in both PNX+DCI and PNX+INF groups compared with *day 0*. Recovery was seen at *day 7* in both groups without statistically significant differences. At *day 14*, the PNX+DCI group and the NoTx group were significantly increased compared with their respective *day 0* values, presumably reflecting adaptation to wheel running, but the PNX+INF group remained at a similar level as *day 7*. The difference at *day 14* was significant between the PNX+DCI group and the PNX+INF group. $*P < 0.05$ vs. respective *day 0* and *day 2* values, $**P < 0.05$ between the indicated groups.

reported to facilitate the movement of coadministered materials into the airway from the nasal orifice (18). Other surface-active materials may also be effective. The delivery of inhaled all-transretinoic acid has been previously reported in detail (17), showing that airway administration is expected to be most efficient in delivering materials to the lung. However, it is possible that systemic concentration of DCI was also significantly elevated in this particular study, since at least a fraction of administered DCI was expected to be absorbed from the nasal mucosa, even with INF. Further delivery and pharmacokinetic studies are necessary to address these issues.

Growth factors such as epidermal growth factor (11), hepatocyte growth factor (27), vascular endothelial growth factor (28), and keratinocyte growth factor (13), and a form of vitamin, retinoic acid (12), have been reported to facilitate compensatory lung growth. Our previous study suggested the importance of TTF-1 in compensatory lung growth (31). The results of the present study indicate that DCI administration augments the induction of TTF-1 after pneumonectomy in the lung in vivo. Although the effect of DCI is likely to be multifaceted, the induction of TTF-1 may, at least in part, be involved in the effects of DCI on facilitating compensatory lung growth, since concomitant administration of TTF-1 siRNAs suppressed the effects of DCI on *day 7*, although this effect was not apparent on *day 2*. It is possible that the induction of TTF-1 by DCI may have peaked earlier than *day 2*. Administration of siRNAs at earlier time points, namely before pneumonectomy, may, to some extent, clarify this issue. Further studies to specify the types of alveolar septal cells affected by DCI are also necessary.

To our knowledge, this is the first report of a material administered through the airway, which facilitates compensatory lung growth. Airway administration would be an ideal route of application in the clinic for materials that are expected to function in the lung. Furthermore, DCI may have advantages over the administration of growth factors in that it is a combination of materials that are clinically accessible and that it is also expected to be more acceptable in terms of cost. Although still preliminary, DCI with further modifications may provide a therapeutic treatment to potentially augment residual lung function after resection.

ACKNOWLEDGMENTS

The authors thank Kei Tsujioka, Division of General Thoracic Surgery, School of Medicine, Keio University, for her expertise in animal experiments.

GRANTS

This work was supported, in part, by grant in aid from the Ministry of Education, Culture, Sports, Science, and Technology-Japan, and the School of Medicine, Keio University fund for the promotion of science.

DISCLOSURES

No conflicts of interest, financial or otherwise are declared by the authors.

REFERENCES

1. **Ad Hoc Statement Committee, American Thoracic Society.** Mechanisms and limits of induced postnatal lung growth. *Am J Respir Crit Care Med* 170: 319–343, 2004.
2. **Ballard PL, Gonzales LW, Williams MC, Roberts JM, Jacobs MM.** Differentiation of type II cells during explant culture of human fetal lung is accelerated by endogenous prostanoids and adenosine 3′,5′-monophosphate. *Endocrinology* 128: 2916–2924, 1991.
3. **Bates SR, Gonzales LW, Tao JQ, Rueckert P, Ballard PL, Fisher AB.** Recovery of rat type II cell surfactant components during primary cell culture. *Am J Physiol Lung Cell Mol Physiol* 282: L267–L276, 2002.
4. **Belloni PN, Garvin L, Mao CP, Bailey-Healy I, Leaffer D.** Effects of all-trans-retinoic acid in promoting alveolar repair. *Chest* 117: 235S–241S, 2000.
5. **Binns OA, DeLima NF, Buchanan SA, Lopes MB, Cope JT, Marek CA, King Laubach VE RC, Tribble CG, Kron IL.** Mature pulmonary lobar transplants grow in an immature environment. *J Thorac Cardiovasc Surg* 114: 186–194, 1997.
6. **Fayon M, Jouvencel P, Carles D, Choukroun ML, Marthan R.** Differential effect of dexamethasone and hydrocortisone on alveolar growth in rat pups. *Pediatr Pulmonol* 33: 443–448, 2002.
7. **Fehrenbach H, Voswinckel R, Michl V, Mehling T, Fehrenbach A, Seeger W, Nyengaard JR.** Neoalveolarisation contributes to compensatory lung growth following pneumonectomy in mice. *Eur Respir J* 31: 515–522, 2008.
8. **Gonzales LW, Guttentag SH, Wade KC, Postle AD, Ballard PL.** Differentiation of human pulmonary type II cells in vitro by glucocorticoid plus cAMP. *Am J Physiol Lung Cell Mol Physiol* 283: L940–L951, 2002.
9. **Inselman LS, Padilla-Burgos LB, Teichberg S, Spencer H.** Alveolar enlargement in obesity-induced hyperplastic lung growth. *J Appl Physiol* 65: 2291–2296, 1988.
10. **Kawakami M, Paul JL, Thurlbeck WM.** The effect of age on lung structure in male BALB/cNNia inbred mice. *Am J Anat* 170: 1–21, 1984.
11. **Kaza AK, Laubach VE, Kern JA, Long SM, Fiser SM, Tepper JA, Nguyen RP, Shockey KS, Tribble CG, Kron IL.** Epidermal growth factor augments postpneumonectomy lung growth. *J Thorac Cardiovasc Surg* 120: 916–921, 2000.
12. **Kaza AK, Kron IL, Kern JA, Long SM, Fiser SM, Nguyen RP, Tribble CG, Laubach VE.** Retinoic acid enhances lung growth after pneumonectomy. *Ann Thorac Surg* 71: 1645–1650, 2001.
13. **Kaza AK, Kron IL, Leuwerke SM, Tribble CG, Laubach VE.** Keratinocyte growth factor enhances post-pneumonectomy lung growth by alveolar proliferation. *Circulation* 106: I120–I124, 2002.
14. **Kida K.** Lack of recovery of lung structure after the administration of beta-amino-propionitrile in the postnatal period. *Am Rev Respir Dis* 122: 467–475. 2002.
15. **Kolla V, Gonzales LW, Gonzales J, Wang P, Angampalli S, Feinstein SI, Ballard PL.** Thyroid transcription factor in differentiating type II cells: regulation, isoforms, and target genes. *Am J Respir Cell Mol Biol* 36: 213–225, 2007.
16. **Laros CD, Westermann CJ.** Dilatation, compensatory growth, or both after pneumonectomy during childhood and adolescence. A thirty-year follow-up study. *J Thorac Cardiovasc Surg* 93: 570–576, 1987.
17. **March TH, Cossey PY, Esparza DC, Dix KJ, McDonald JD, Bowen LE.** Inhalation administration of all-trans-retinoic acid for treatment of elastase-induced pulmonary emphysema in Fischer 344 rats. *Exp Lung Res* 30: 383–404, 2004.
18. **Massaro D, Massaro GD, Clerch LB.** Noninvasive delivery of small inhibitory RNA and other reagents to pulmonary alveoli in mice. *Am J Physiol Lung Cell Mol Physiol* 287: L1066–L1070, 2004.
19. **Massaro GD, Mortola JP, Massaro D.** Sexual dimorphism in the architecture of the lung's gas-exchange region. *Proc Natl Acad Sci USA* 92: 1105–1107, 1995.
20. **Massaro GD, Mortola JP, Massaro D.** Estrogen modulates the dimensions of the lung's gas-exchange surface area and alveoli in female rats. *Am J Physiol Lung Cell Mol Physiol* 270: L110–L114, 1996.
21. **Massaro GD, Massaro D.** Postnatal treatment with retinoic acid increases the number of pulmonary alveoli in rats. *Am J Physiol Lung Cell Mol Physiol* 270: L305–L310, 1996.
22. **Massaro GD, Massaro D.** Retinoic acid treatment partially rescues failed septation in rats and in mice. *Am J Physiol Lung Cell Mol Physiol* 278: L955–L960, 2000.
23. **Morani A, Barros RP, Imamov O, Hultenby K, Arner A, Warner M, Gustafsson JA.** Lung dysfunction causes systemic hypoxia in estrogen receptor beta knockout (ERβ-/-) mice. *Proc Natl Acad Sci USA* 103: 7165–7169, 2006.
24. **Nakajima C, Kijimoto C, Yokoyama Y, Miyakawa T, Tsuchiya Y, Kuroda T, Nakano M, Saeki M.** Longitudinal follow-up of pulmonary function after lobectomy in childhood—factors affecting lung growth. *Pediatr Surg Int* 13: 341–345, 1988.

25. **Rannels DE, Karl HW, Bennett RA.** Control of compensatory lung growth by adrenal hormones. *Am J Physiol Endocrinol Metab* 253: E343–E348, 1987.
26. **Sahebjami H, Domino M.** Effects of postnatal dexamethasone treatment on development of alveoli in adult rats. *Exp Lung Res* 15: 961–973, 1989.
27. **Sakamaki Y, Matsumoto K, Mizuno S, Miyoshi S, Matsuda H, Nakamura T.** Hepatocyte growth factor stimulates proliferation of respiratory epithelial cells during postpneumonectomy compensatory lung growth in mice. *Am J Respir Cell Mol Biol* 26: 525–533, 2002.
28. **Sakurai MK, Lee S, Arsenault DA, Nose V, Wilson JM, Heymach JV, Puder M.** Vascular endothelial growth factor accelerates compensatory lung growth after unilateral pneumonectomy. *Am J Physiol Lung Cell Mol Physiol* 292: L742–L747, 2007.
29. **Scherle W.** A simple method for volumetry of organs in quantitative stereology. *Mikroskopie* 26: 57–60, 1970.
30. **Schultz H, Johner C, Edger G, Ziesenis A, Reitmeier P, Heyder J, Balling R.** Respiratory mechanics in mice: strain and sex specific differences. *Acta Physiol Scand* 174: 367–375, 2002.
31. **Takahashi Y, Izumi Y, Kohno M, Kimura T, Kawamura M, Okada Y, Nomori H, Ikeda E.** Thyroid transcriprion factor 1 influences the early phase of compensatory lung growth in adult mice. *Am J Respir Crit Care Med* 181: 1397–1406.
32. **Ueda K, Tanaka T, Hayashi M, Li TS, Tanaka N, Hamano K.** Computed tomography-defined functional lung volume after segmentectomy versus lobectomy. *Eur J Cardiothorac Surg* 37: 1433–1437, 2010.
33. **Voswinckel R, Motejl V, Fehrenbach A, Wegmann M, Mehling T, Fehrenbach H, Seeger W.** Characterisation of post-pneumonectomy lung growth in adult mice. *Eur Respir J* 24: 524–532, 2004.
34. **Weibel ER.** *Stereological Methods.* New York: Academic, 1979, p. 9–196.
35. **Weibel ER.** Biomorphometry in physiological and pathological research. *Acta Med Pol* 23: 115–125, 1982.
36. **Zhang X, Shan P, Jiang D, Noble PW, Abraham NG, Kappas A, Lee PJ.** Small interfering RNA targeting heme oxygenase-1 enhances ischemia-reperfusion-induced lung apoptosis. *J Biol Chem* 279: 10677–10684, 2004.

Cryobiology 61 (2010) 317–326

Contents lists available at ScienceDirect

Cryobiology

journal homepage: www.elsevier.com/locate/ycryo

On freeze-thaw sequence of vital organ of assuming the cryoablation for malignant lung tumors by using cryoprobe as heat source ☆

Seishi Nakatsuka [a], Hideki Yashiro [b], Masanori Inoue [a], Sachio Kuribayashi [a], Masafumi Kawamura [c,d], Yotaro Izumi [c], Norimasa Tsukada [e], Yoshikane Yamauchi [c], Kohei Hashimoto [c], Kansei Iwata [f], Taisuke Nagasawa [f,*], Yi-Shan Lin [f]

[a] Department of Diagnostic Radiology, School of Medicine, KEIO University, 35 Shinanomachi, Shinjuku-ku, Tokyo 160-8582, Japan
[b] Hiratsuka City Hospital, 1-19-1 Minamihara, Hiratsuka, Kanagawa 254-0065, Japan
[c] Division of General Thoracic Surgery, School of Medicine, KEIO University, 35 Shinanomachi, Shinjuku-ku, Tokyo 160-8582, Japan
[d] Division of General Thoracic Surgery, School of Medicine, TEIKYO University, 2-11-1 Kaga, Itabashi-ku, Tokyo 173-0003, Japan
[e] Kawasaki Municipal Hospital, Shinkawadori, Kawasaki-ku, Kawasaki, Kanagawa 210-0013, Japan
[f] DgS Computer Co., Ltd., 2-27 Minamiosawa, Hachioji, Tokyo 192-0364, Japan

ARTICLE INFO

Article history:
Received 8 April 2010
Accepted 18 October 2010
Available online 29 October 2010

Keywords:
Freezing function
Freeze-thaw sequence
Isothermal curve
Cryosurgery
Cryoablation
Lung cancer
Joule–Thomson effect
Porcine lung

ABSTRACT

Regarding cryoablation for the malignant lung tumors, multiple trials of the freeze-thaw process have been made, and we considered it necessary to view and analyze the freeze-thaw process as a freeze-thaw sequence. We caused the sequence in a porcine lung *in vivo* by using an acicular, cylindrical stainless-steel probe as the heat source for the freeze-thaw sequence and cooling to −150 °C with super high-pressure argon gas by causing the Joule–Thomson effect phenomenon at the tip of the probe. In this experiment, we examined the sequence by measuring the temperature and using the isothermal curve and the freezing function. As a result, it was demonstrated that the freezing characteristics considerably differed in the first sequence and the second sequence from those of non-aerated organs such as liver and kidney. In our experiments on porcine lung, thermal properties were considered to change as the bleeding caused by the first thawing infiltrated in the lung parenchyma, and it was confirmed that the frozen area in the second cycle was dramatically enlarged as compared with the first cycle (when a similar sequence is continuously repeated, we say it as cycle). This paper provides these details.

The cryoablation for the malignant lung tumors is a treatment to cause local cell necrosis by a rapid freezing/thawing at the tip of the cryoprobe. Percutaneous cryoablation of lung tumors by using the Joule–Thomson effects with high-pressure argon gas and high-pressure helium gas has been safely performed under CT fluoroscopic guidance in our institute [1,2]. A cycle of the 5–10 min freezing and the thawing creates the frozen area, which was enlarged after repetition of the cycles.

There have been a large number of studies about cryoablation [3], but there are few experimental studies about the lung cryoablation [4–7]. We have made both theoretical and experimental analyses about the enlargement of the freezing surface of a normal porcine lung in order to necrose cells infallibly during cryoablation [8,9]. In this connection, we have conducted the prediction of the freezing progress in lung tumors by using a two-dimensional heat conduction analysis with an enthalpy method and a one-dimensional heat conduction analysis with an approximation equation. The results of these two methods gave similar results. We made a theoretical prediction that there was a limit (limiting radius) to an iceball *in vivo* or a freezing limitation due to the heat balance between the cryogenic temperature of the cryoprobe as a cryogen and the heat source of the surrounding area. In the experiments, on the other hand, we conducted each trial of freezing on a porcine lung with a cryoprobe and measured the size of a frozen area. As a result, we confirmed that the theoretical calculation used in the previous paper [9] on the freezing curve reproduced the experimental values. To analyze the freezing characteristics such as the limiting radius, we defined the freezing function $f(t)$ of time t indicating the radius of freezing surface of the iceball as follows:

$$f(t) = a\exp(bt) + c(a, b < 0, c > 0). \quad (1)$$

Then, we fitted free parameters, a, b and c, to experimental data with the least-square method. Although freezing function is a nonlinear function, when the time is infinite, its first term becomes zero and freezing function converges to the intercept c which is equivalent to the value of the limiting radius of the iceball. As a

☆ *Statement of funding:* This work was supported by Grant-in-Aid for Scientific Research (21591823) of the Japanese Ministry of Education, Culture, Sports, Science and Technology (MK).

* Corresponding author.
E-mail address: nagasawa@dgs.co.jp (T. Nagasawa).

0011-2240/$ - see front matter © 2010 Elsevier Inc. All rights reserved.
doi:10.1016/j.cryobiol.2010.10.157

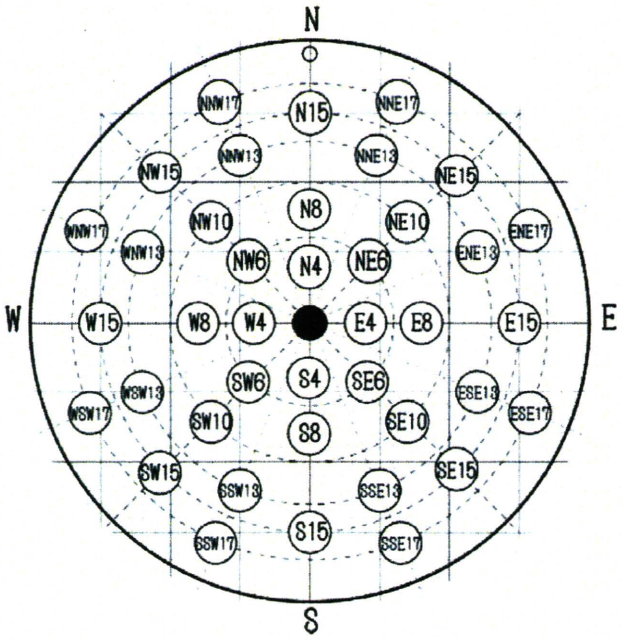

Fig. 1. Positions of the cryoprobe (center) and the thermocouples. N, E, S, and W stand for North, East, South and West, respectively and the numbers indicate the distance (mm) from the center, where the cryoprobe is positioned.

result of the analysis using this freezing function, it was found that the iceball reaches the equilibrium state in approximately 300 s at single freezing of the posterior lobe of the porcine lung and the measured limiting radius was about 10 mm. In order to verify the effectiveness of multiple cycles in cryoablation for malignant lung tumors, we conducted triple freeze-thaw cycle using the cryoprobe; one or two places per swine at the normal posterior lobe of lung, or 10 places in total. A set of 40 thermocouples located around the cryoprobe were used for temperature measurement. A temperature simulation model is proposed and thereby allows real-time monitoring of the temperature behavior during a treatment of cryoablation. Moreover, the freeze-thaw sequence was analyzed by using the freezing function indicated in Eq. (1).

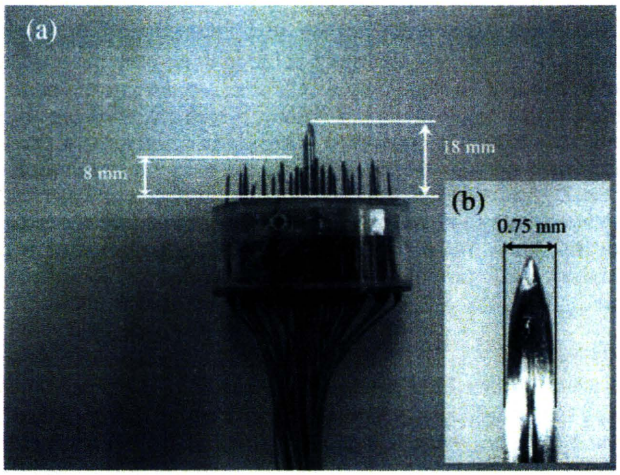

Fig. 2. (a) The cryoprobe and the measurement device. The cryoprobe at the center and the thermocouples are fixed at 18 and 8 mm from the tip of each for the depth of puncture in the porcine lung. (b) The tip of a thermocouple. The alumel wire and the chromel wire are connected only at the tip.

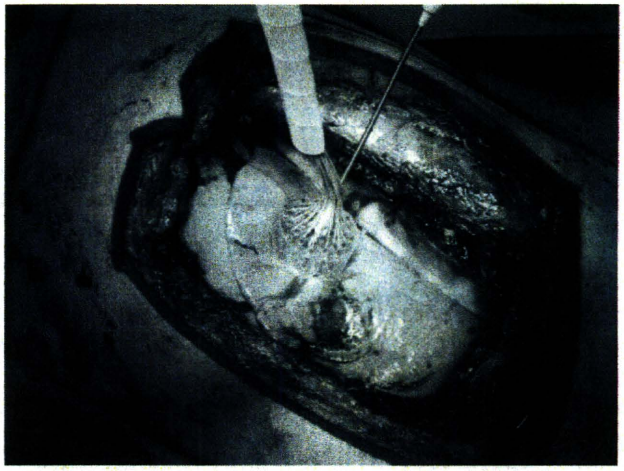

Fig. 3. The picture showing how the temperature is measured. Cryoprobe and thermocouples are inserted by pressing the measurement device to the posterior lobe of lung.

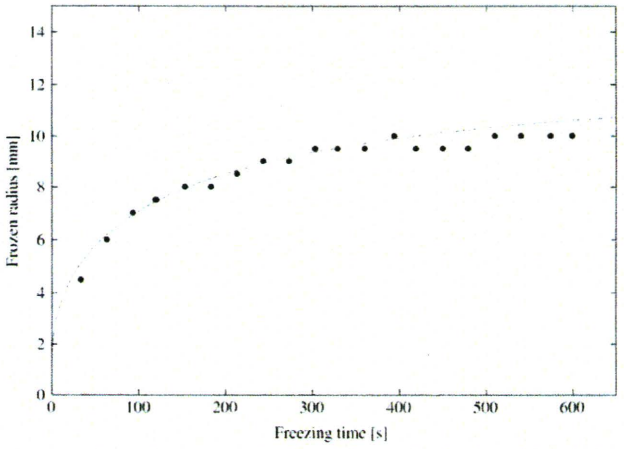

Fig. 4. Comparison of the frozen radius between the experimental data (dot) and the analytical solution (line). Freezing curve by the analytical solution is calculated by using the parameter set 2 in Table 3 except $\omega_{eff} = 0.04$. The experimental data originate from [8].

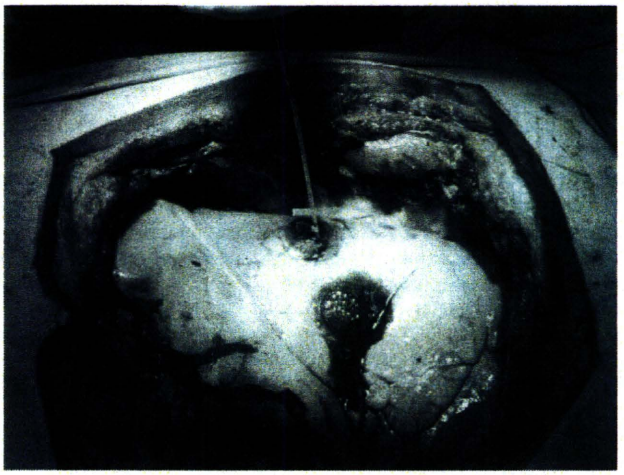

Fig. 5. Bleeding around the cryoprobe at the first thawing. The freeze-thaw cycle was completed three times at the other bleeding spot below.

Furthermore, we conducted three cases of the double freeze-thaw cycle with the swine liver to compare with the lung cases, and analyzed the freeze-thaw sequence with the isothermal curve and the freezing function in the same manner as the lung cases. Also, we conducted one case of the double freeze-thaw cycle with the swine kidney, and analyzed the freeze-thaw sequence by examining the temperature change.

Methods

Experiment

We carried out the experiments for 10 male swine (3 months old, approximately 40 kg of weight) on the posterior lobe of lung using a 2.4-mm cryoprobe for freezing (Endocare, Irvine, USA), after exposing the right lung under general anesthesia and respiration control with a ventilator. *K*-type thermocouples were used for temperature measurement. Measurements were conducted at every 5 s for 40 points at the same time by using a data logger (Pico Technology, UK). A 2.4-mm cryoprobe was inserted at the center, and four thermocouples each at 4, 6, 8 and 10 mm positions from the center and eight thermocouples each at 13, 15 and 17 mm positions from the center were fixed by using an acrylic device (Yokohama Micro Giko, Japan; Fig. 1). Since, however, the positions of thermocouples can be inaccurate due to design limitation, the lengths of radius are separately measured for accuracy. We found, in advance, that the largest radius of the iceball was generated by freezing in egg white approximately 10 mm from the tip of the cryoprobe. To measure the temperature change at the position of the largest freezing capability of a cryoprobe, the cryoprobe and thermocouples were fixed at 18 and 8 mm from the tip of each for the depth of puncture in the porcine lung (Fig. 2(a)). The tip of the thermocouple is very thin as shown in Fig. 2(b), the chromel wire and the alumel wire are connected at the tip only and the influence of the thermocouple temperature measurements was minimized. Fig. 3 shows how the cryoprobe is inserted actually and the temperature is measured. Three cycles of freeze-thaw experiments were conducted for each puncture point. Like clinical experiences of lung, the freeze-thaw cycle was set for the freezing time of 5 min for the first freezing and 10 min for the second and the third freezing. The past studies showed that the equilibrium state was reached in about 300 s in the first freezing [8]. Thawing progresses until the temperature measured by the thermocouple in the cryoprobe, reaches 30 or 20 °C with the use of high-pressure helium gas (active thawing); the helium gas is then stopped (passive thawing) for the first and the second thawing, which takes

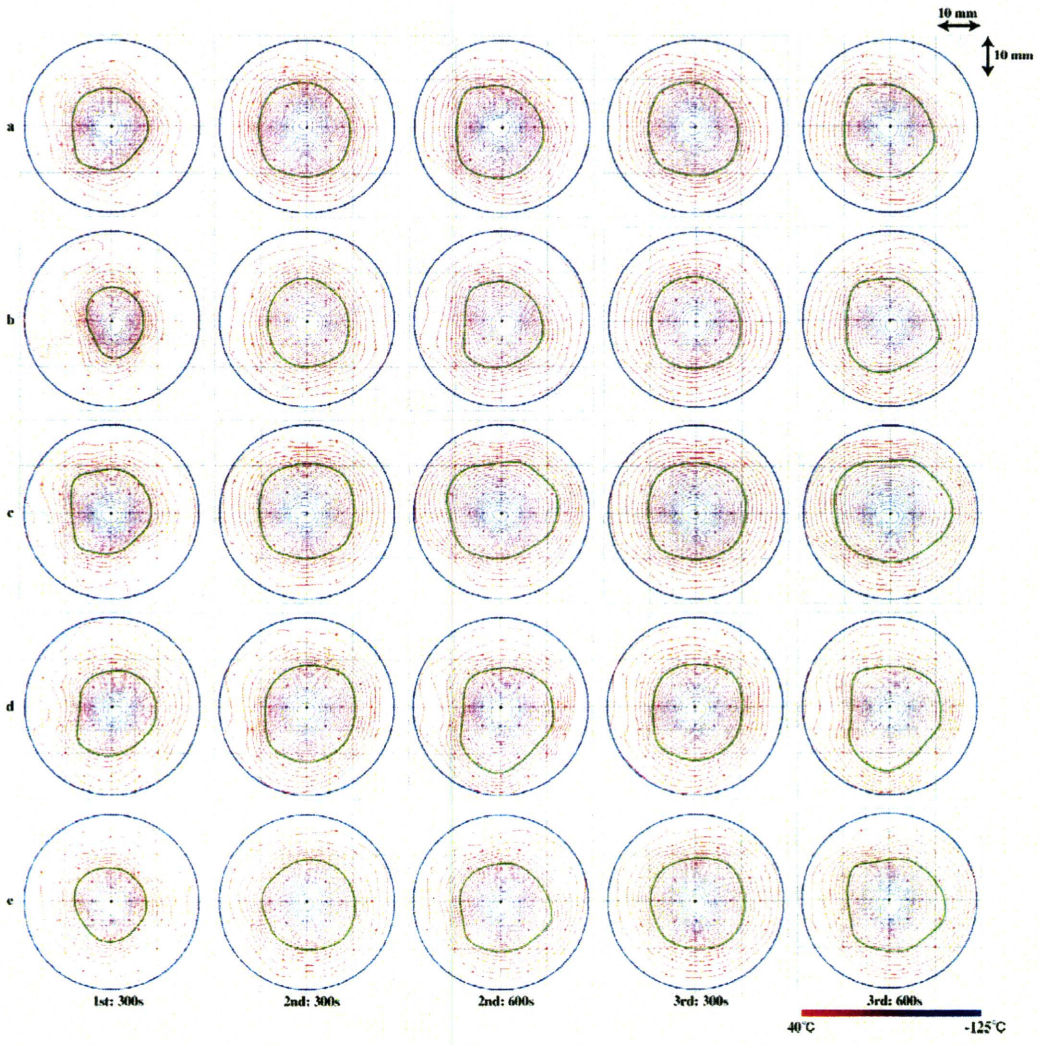

Fig. 6a. Isothermal curves in the experiments of lung (active thawing 30 °C). The green curves show freezing temperature. Each interval between the isothermal curves is 5 °C. (For interpretation of the references to colour in this figure legend, the reader is referred to the web version of this article.)

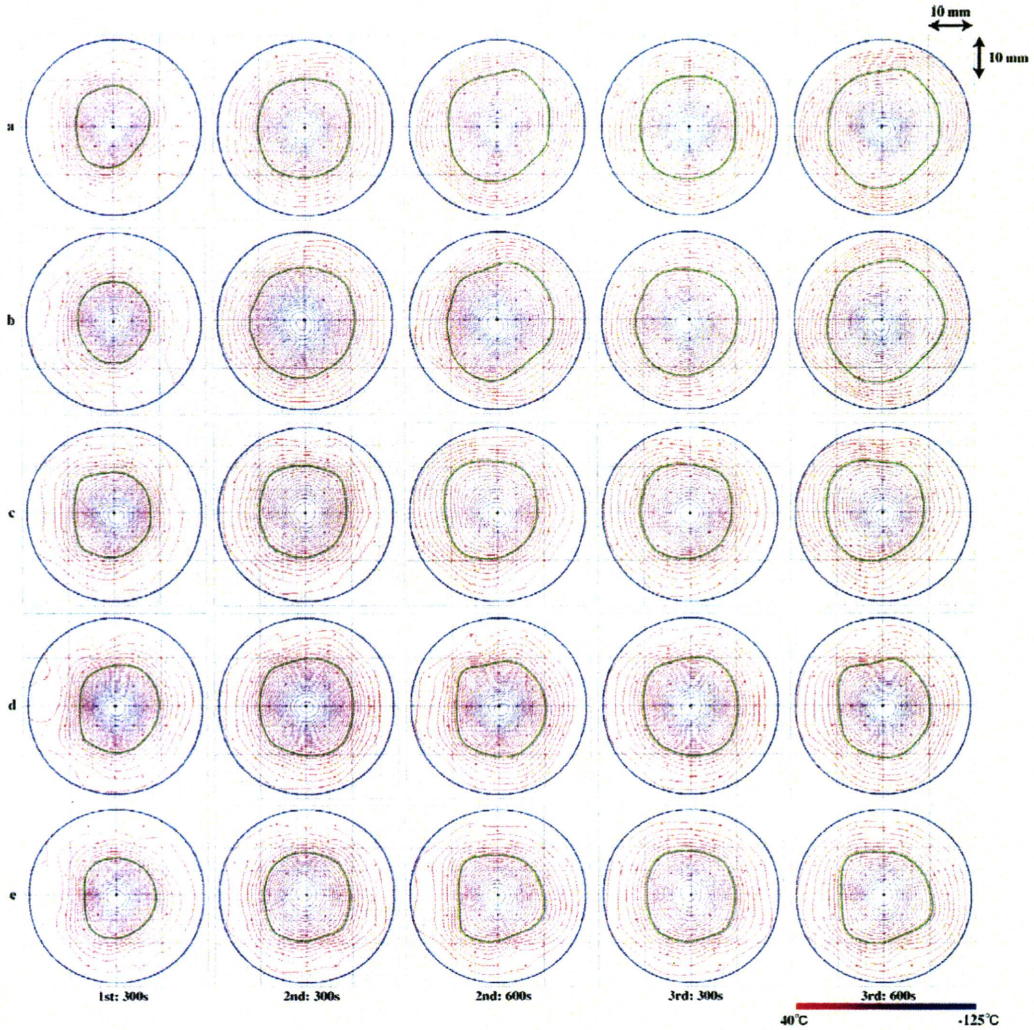

Fig. 6b. Isothermal curves in the experiments of lung (active thawing 20 °C). The notation is the same as in the figure (a).

10 min in total; for the third thawing, high-pressure helium gas is used until the cryoprobe is removed, which is the end of the work. All animal studies were approved by the School of Medicine, Keio University, Institutional Animal Care and Use Committee, and were carried out in accordance with the "Guide for the Care and Use of Laboratory Animals" published by the National Institute of Health.

Theoretical analysis

The analytical solution used here is based on the following one-dimensional governing equation within a living organism [9]:

$$\rho_s c_s \frac{\partial T}{\partial t} = \frac{1}{r}\frac{\partial}{\partial r}\left(r k_s \frac{\partial T}{\partial r}\right) + \rho_f c_f \omega_{\text{eff}}(T_f - T) + S_m. \tag{2}$$

Here, r and T stand for position and temperature, respectively. Also, c and k are density, specific heat and thermal conductivity, respectively, and their subscripts, s and f show tissue and blood. S_m is the metabolic heat generation and ω_{eff} is the effective perfusion rate which we introduced and it is a semi-empirical value. The boundary conditions for the freezing process using the cryoprobe of outer radius R_p are given as follows:

$$\begin{aligned} &T = T_p: \quad (0 \leqslant r \leqslant R_p), \\ &T = T_0: \quad (R_m \leqslant r), \end{aligned} \tag{3}$$

where R_m is the radius from the point of which temperature is body temperature T_0. The following equation can be obtained from the energy balance relationship at the freezing point $r = R_i$:

$$\rho_i h_{sf} R_i \frac{dR_i}{dt} = R_i k_i \left.\frac{\partial T}{\partial r}\right|_{r=R_i} - R_i k_c \left.\frac{\partial T}{\partial r}\right|_{r=R_i} - \rho_c c_c (T_0 - T_i) R_i \frac{dR_i}{dt}. \tag{4}$$

Here, h_{sf} indicates latent heat of solidification and the subscripts i and c stand for frozen region and non-frozen region. A quasi-steady approximation works out for the first term on the right-hand side which shows heat flux from the frozen region as long as freezing speed is not extremely fast, and the temperature in the frozen region can be shown as follows:

$$\frac{T - T_p}{T_i - T_p} = \frac{\ln(r/R_p)}{\ln(R_i/R_p)}: \quad R_p \leqslant r \leqslant R_i. \tag{5}$$

The first term on the right-hand side of Eq. (4) is

$$R_i k_i \left.\frac{\partial T}{\partial r}\right|_{r=R_i} = k_i \frac{T_i - T_p}{\ln(R_i/R_p)}. \tag{6}$$

In the same way, let us assume that the second term on the right-hand side which shows heat flux from non-frozen region can be shown as the following equation that satisfies the temper-

ature of the non-frozen region $T = T_i$ with boundary condition of $r = R_i$ and also $T = T_0$ and $\partial T/\partial r = 0$ with boundary condition of $r = R_m$:

$$\frac{T - T_0}{T_i - T_0} = \left(1 - \frac{r - R_i}{R_m - R_i}\right)^2 : \quad R_i \leqslant r \leqslant R_m. \tag{7}$$

Under quasi-steady approximation, the Eq. (2) is integrated to give:

$$-k_c R_i \left.\frac{dT}{dr}\right|_{r=R_i} - \rho_c c_c \omega_{\text{eff}} \int_{R_i}^{R_m} r(T - T_0)dr + S_m \int_{R_i}^{R_m} r dr = 0. \tag{8}$$

Substituting the Eq. (7) into the Eq. (8):

$$2k_c R_i \frac{T_i - T_0}{R_m - R_i} - \rho_c c_c \omega_{\text{eff}}(T_i - T_0)\left[\frac{1}{3}(R_m - R_i)R_i + \frac{1}{12}(R_m - R_i)^2\right] + S_m \frac{R_m^2 - R_i^2}{2} = 0, \tag{9}$$

which is derived and forms a cubic equation for $R_i/(R_m - R_i)$. Based on Newton's shooting method, the following explicit expression gives a quite accurate value for the root:

$$\frac{R_i}{R_m - R_i} = R_i \sqrt{\frac{1}{6}\left[\frac{\omega_{\text{eff}}}{\alpha_c} + 3\frac{S_m}{k_c(T_0 - T_i)}\right]} + \frac{1}{8}\left[\frac{\frac{\omega_{\text{eff}}}{\alpha_c} + 6\frac{S_m}{k_c(T_0 - T_i)}}{\frac{\omega_{\text{eff}}}{\alpha_c} + 3\frac{S_m}{k_c(T_0 - T_i)}}\right], \tag{10}$$

where $\alpha = k/\rho c$ is the thermal diffusivity. As a result, the second term on the right-hand side of the Eq. (4) is given by using the Eqs. (7) and (10):

$$k_c R_i \left.\frac{dT}{dr}\right|_{r=R_i} = 2k_c(T_0 - T_i)\left\{R_i \sqrt{\frac{1}{6}\left[\frac{\omega_{\text{eff}}}{\alpha_c} + 3\frac{S_m}{k_c(T_0 - T_i)}\right]} + \frac{1}{8}\left[\frac{\frac{\omega_{\text{eff}}}{\alpha_c} + 6\frac{S_m}{k_c(T_0 - T_i)}}{\frac{\omega_{\text{eff}}}{\alpha_c} + 3\frac{S_m}{k_c(T_0 - T_i)}}\right]\right\}. \tag{11}$$

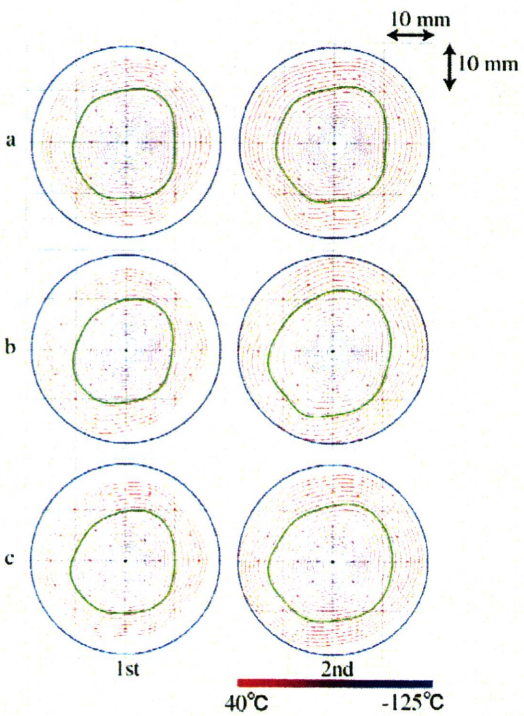

Fig. 7. Isothermal curves in the experiments of liver. The notation is the same as in the Fig. 6a. Curves reach the equilibrium state at both the first and the second time freezing.

Finally, by substituting the Eqs. (6) and (11) into the Eq. (3), it can be shown as following:

$$dt^* = \frac{1 + \text{Sr}}{\text{Ste}} \frac{R_i^* \ln R_i^*}{1 - \frac{\ln R_i^*}{\text{Cr}}\left[\sqrt{\frac{2}{3}(\omega^* + 3\text{Met})^{1/2} R_i^* + \frac{\omega^* + 6\text{Met}}{4(\omega^* + 3\text{Met})}}\right]} dR_i^*. \tag{12}$$

Here, the following dimensionless parameters are introduced:

$$R_i^* = R_i/R_p, \tag{13a}$$

$$t^* = \alpha_l t/R_p^2, \tag{13b}$$

$$\text{Ste} = \frac{c_l(T_i - T_p)}{h_{sf}}, \tag{13c}$$

$$\text{Sr} = \frac{\rho_c c_c (T_0 - T_i)}{\rho_l h_{sf}}, \tag{13d}$$

$$\omega^* = \frac{\omega_{\text{eff}} R_p^2}{\alpha_c}, \tag{13e}$$

$$\text{Cr} = \frac{k_l(T_i - T_p)}{k_c(T_0 - T_i)}, \tag{13f}$$

$$\text{Met} = \frac{S_m R_p^2}{k_c(T_0 - T_i)}. \tag{13g}$$

In above definitions (Eqs. (13a)–(13g)), ω^* and Cr correspond to β and ϕ of Cooper and Trezek [10], respectively. The analytical solution can be obtained by solving the differential Eq. (12) by numerical calculation. The quasi-steady assumption is valid when $t^*\text{Ste}/(1 + \text{Sr}) > 1$, which roughly gives $t > 1$ s. Thus, the assumption holds for most parts of the freezing process except at its initial short period.

Fig. 4 shows the comparison of the time variation of the frozen radius between the experimental data and this analytical solution. It is found that, as time advances, the analytical solution overestimates the frozen radius. This defect may be partially due to neglect of the axial term.

Results

In the first thawing, the bleeding from the frozen region was confirmed (Fig. 5). The frozen area in the second thawing was visibly larger than that of the first thawing.

In order for real-time monitoring of the temperature distribution around the cryoprobe, a set of thermocouples is settled around the cryoprobe for temperature measurement purpose. These scattered temperature data are then interpolated by the Radial Basis

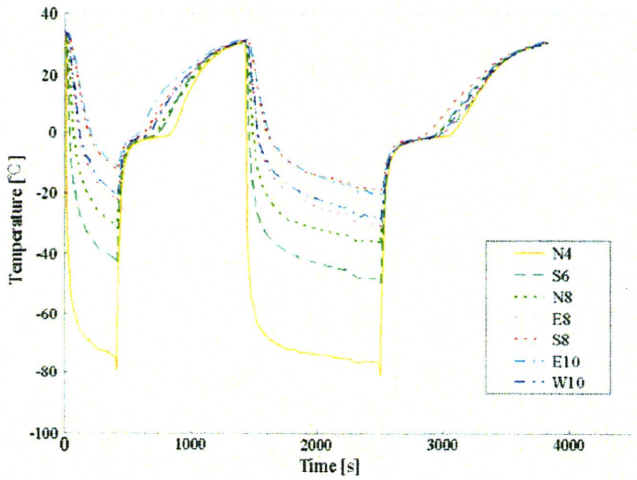

Fig. 8. Temperature change in the experiment of kidney.

Function Interpolation method [11] where the radial function is defined as

$$\phi(r) = |r|^{3/2} \cdot \ln r. \tag{14}$$

Based on the n measurements, the following interpolated function is used to describe the temperature behavior with n radial basis functions:

$$f(x) = \sum_{i=1}^{n} \omega_i \cdot \phi(\|x - c_i\|), \tag{15}$$

where c_i is the position of the ith measured point and ω_i is the weight associated to the radial basis function centered at c_i. The weighting term could be derived by solving the following system of equations:

$$\begin{bmatrix} \phi_{11} & \phi_{12} & \cdots & \phi_{1n} \\ \phi_{21} & \phi_{22} & \ddots & \phi_{2n} \\ \vdots & \vdots & \ddots & \vdots \\ \phi_{n1} & \phi_{n2} & \cdots & \phi_{nn} \end{bmatrix} \begin{bmatrix} \omega_1 \\ \omega_2 \\ \vdots \\ \omega_n \end{bmatrix} = \begin{bmatrix} T_1 \\ T_2 \\ \vdots \\ T_n \end{bmatrix}, \tag{16}$$

where ϕ_{ij} denotes $\phi(\|c_i - c_j\|)$ and T_i is the measured temperature at c_i. Based on the interpolated function, the overall temperature distribution around the cryoprobe could be derived. Finally, in order to provide for user visualization, the distribution of temperature is

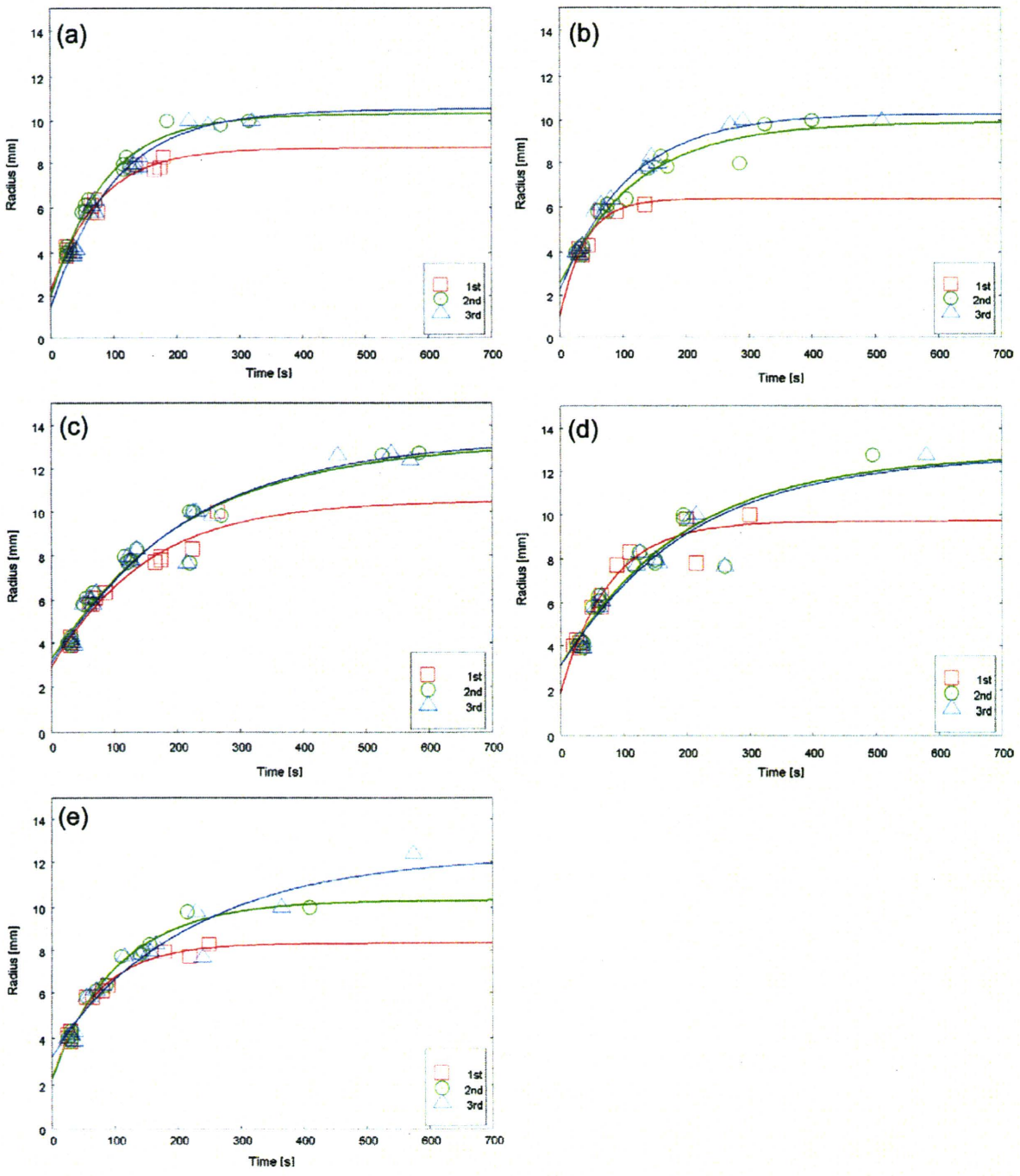

Fig. 9a. Freezing function in the experiments of lung (active thawing 30 °C).

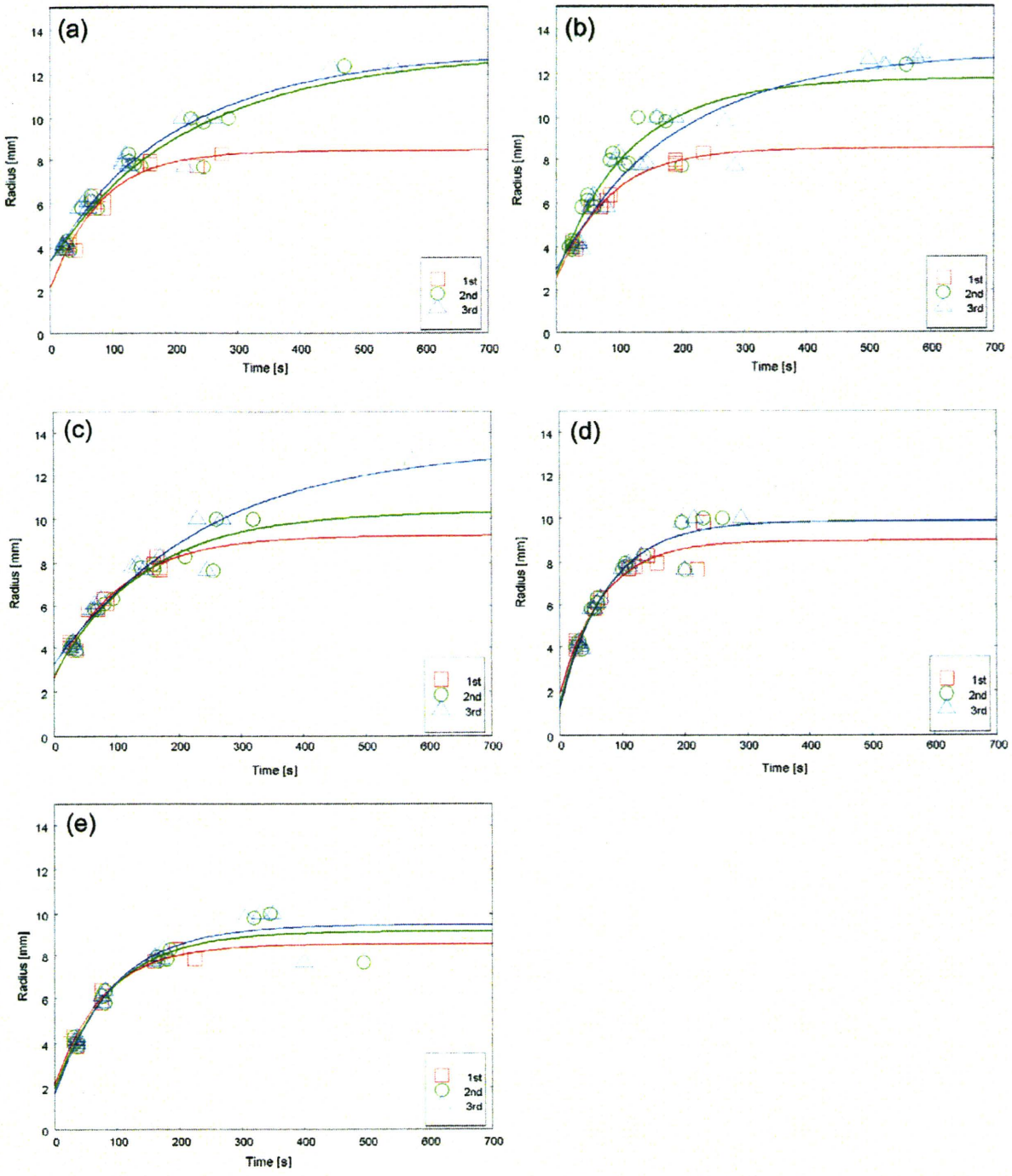

Fig. 9b. Freezing function in the experiments of lung (active thawing 20 °C).

presented by the isothermal plot where the locations with the same temperature are found and connected by Cubic B-Spline functions.

In the experiment, the freeze-thaw sequence was repeated three times, and the isothermal curves at each time of freeze termination are shown in Fig. 6.

The isothermal curve of the first freezing is generally deformed as deviating from the concentric circle, but the isothermal curves in the second and the third freezing are similar to each other and are circular as compared with the one of the first freezing. Comparing each frozen area after 300 s, it was found that the frozen areas of the second and the third cycles are obviously larger than that of first cycle. From the temperature change in each cycle, the second cycle or later apparently provides more freezing than the first cycle. In addition, it was known that the difference between the second cycle and the third cycle was smaller than the difference between the first cycle and the second cycle.

The following shows the comparison with other organs. The temperature was measured at 32 places of three cases of liver, and two cycles of freeze-thaw experiments were conducted. Unlike lung experiments, the first freezing did not reach the equilibrium state in 300 s in the case of liver. The freeze-thaw cycle of liver experiments was different from that of lung experiments in the point that freezing and thawing were both switched when the equilibrium state was reached. Fig. 7 shows the isothermal curve

of each case. The frozen area grew in the shape of a concentric circle and to about 10 mm in the equilibrium state of the first freezing. At the equilibrium state of the second freezing, the frozen area shows the temperature distribution in a similar shape as compared with the first freezing, but it did not grow dramatically larger in size. In comparison with the experiments of lung, the changes in the temperature or diameter curves observed in the experiments of the liver are found that it is similar to the change from the second freezing to the third of lung.

The temperature was measured at 7 places of one kidney, and two cycles of freeze-thaw experiment was conducted. Fig. 8 shows the temperature change in the experiment of kidney. It is found that the temperature changes at all the 7 places in the first cycle and the second cycle were almost the same. Therefore, it can be said that the changes of isothermal curves of kidney and liver are similar in the freeze-thaw sequence.

Discussion

We applied the least-square method (Marquardt–Lovenberg algorithm) to each of the 10 cases of the experiment to obtain the freezing function as Eq. (1) by plotting the freezing time for each thermocouple based on the experiment values of the radius of the thermocouple to the cryoprobe.

The freezing function is shown in Figs. 9a and 9b. It is clearly noted that the curves in the second and the third freezing have a larger radius than the curve in the first freezing.

The values of the free parameters, a, b and c, obtained by the least-square method are as shown in Table 1. Regarding all the 10 cases of experiment, it is found that the value of the limiting radius, c, is greater in the second and the third freezing than in the first freezing and the value b indicating the curvature is smaller in the first freezing than in the others. Although the duration of the freezing are different between the first freezing and the second and the third freezing, this shows that the second and the third freezing provide a dramatically larger frozen area than the first freezing. On the other hand, the difference in the size of the frozen area between the second freezing and the third freezing is less pronounced than the one between the first freezing and the second freezing.

When compared with the liver, the freezing function in the experiments of liver is almost same in the first freezing and the second freezing as shown in Fig. 10. Table 2 shows the free parameters obtained by the least-square method. It is found that the values, a, b and c, do not dramatically change from the first freezing to the second freezing, which is much different from the lung experiments. Regarding the liver as non-aerated organ, the first cycle did not cause a dramatic change in the thermal properties. Therefore, it is considered that the iceball hardly grows in the first and the second cycles. In the meantime, in the lung experiments, the pathological structure and the thermal properties drastically change between the first cycle and the second cycle. Between the second cycle and the third cycle, it is supposed that the thermal properties have no change like non-aerated organs.

Fig. 11 shows the freezing curves obtained from the analytical solution using the parameters shown in Table 3 . As far as the parameters used, thermal conductivity is greater in the parameter set 2 than in the parameter set 1, and so is density. As the graph shows, the difference in the frozen area arises as time advances, and it is found that the frozen area is greater in the parameter set 2.

According to a paper on the pathological change after lung cryoablation reported by Izumi et al. [4], it is considered that infiltration of the blood from the frozen region into the aerated lung parenchyma during the first freezing has a profound effect on increasing thermal conductivity by pushing out the air. As a result, the frozen area in the second cycle is possibly greater than the one in the first cycle. On the other hand, in the second and later cycles, since there is no change in the area where once blood infiltrated it is considered that the thermal properties do not change as in non-aerated organs and that the frozen area does not grow dramatically large. Two types of active thawing up to 20 and up to 30 °C followed by passive thawing were done. No obvious differences in temperature curves could be found. Thawing still remains to be a challenge for the future.

In some papers on animal experiments of hepatic or renal cryoablation, the iceball volume at the end of the second freezing cycle was significantly larger than the volume at the end of the first freezing [12–14]. In another paper on cryoablation for sheep liver, the zone of necrosis as a percentage of the original iceball diameter was significantly higher following a double freeze-thaw cycle [15], which is supported by a paper on the temporary elevation of serum transaminase level after hepatic cryoablation [16]. For non-aerated organs, the double freeze-thaw cycle may thus facilitate tumor destruction and is recommended. This study suggests that the first freezing cycle is just to create optimal environment for heat conduction, the second is to produce larger iceball and the third may be necessary for more effective cytotoxicity. This result supports the fact that the triple freeze-thaw cycle has been applied in our clinical experience of pulmonary cryoablation [1].

Conclusion

We drew the isothermal curves by measuring the temperature of a normal porcine lung *in vivo* based on the same freeze-thaw cycles as actual cryoablation for malignant lung tumors. Further-

Table 1
Parameters for freezing function, $f(t) = a\exp(bt) + c$, in the experiments of lung obtained by the least-square method. 30 and 20 in the first column indicate active thawing up to 30 and 20 °C, respectively.

		a	$b \times 10^2$	c
30a	1st	−6.48	−1.29	8.71
	2nd	−8.29	−1.13	10.32
	3rd	−9.08	−0.99	10.54
30b	1st	−5.35	−2.61	6.34
	2nd	−7.32	−0.79	9.90
	3rd	−8.03	−0.89	10.31
30c	1st	−7.65	−0.67	10.50
	2nd	−9.95	−0.46	13.22
	3rd	−10.29	−0.46	13.37
30d	1st	−7.87	−1.32	9.69
	2nd	−9.72	−0.50	12.83
	3rd	−9.70	−0.49	12.78
30e	1st	−6.05	−1.32	8.34
	2nd	−8.05	−0.93	10.31
	3rd	−9.08	−0.47	12.29
20a	1st	−6.32	−1.24	8.45
	2nd	−9.53	−0.45	12.91
	3rd	−9.57	−0.49	12.98
20b	1st	−5.97	−1.18	8.51
	2nd	−9.09	−0.85	11.79
	3rd	−9.97	−0.52	12.94
20c	1st	−6.63	−0.98	9.24
	2nd	−7.60	−0.70	10.33
	3rd	−10.08	−0.41	13.34
20d	1st	−7.09	−1.50	8.96
	2nd	−8.46	−1.34	9.86
	3rd	−8.65	−1.36	9.85
20e	1st	−6.42	−1.25	8.52
	2nd	−7.20	−1.07	9.16
	3rd	−7.77	−1.05	9.47

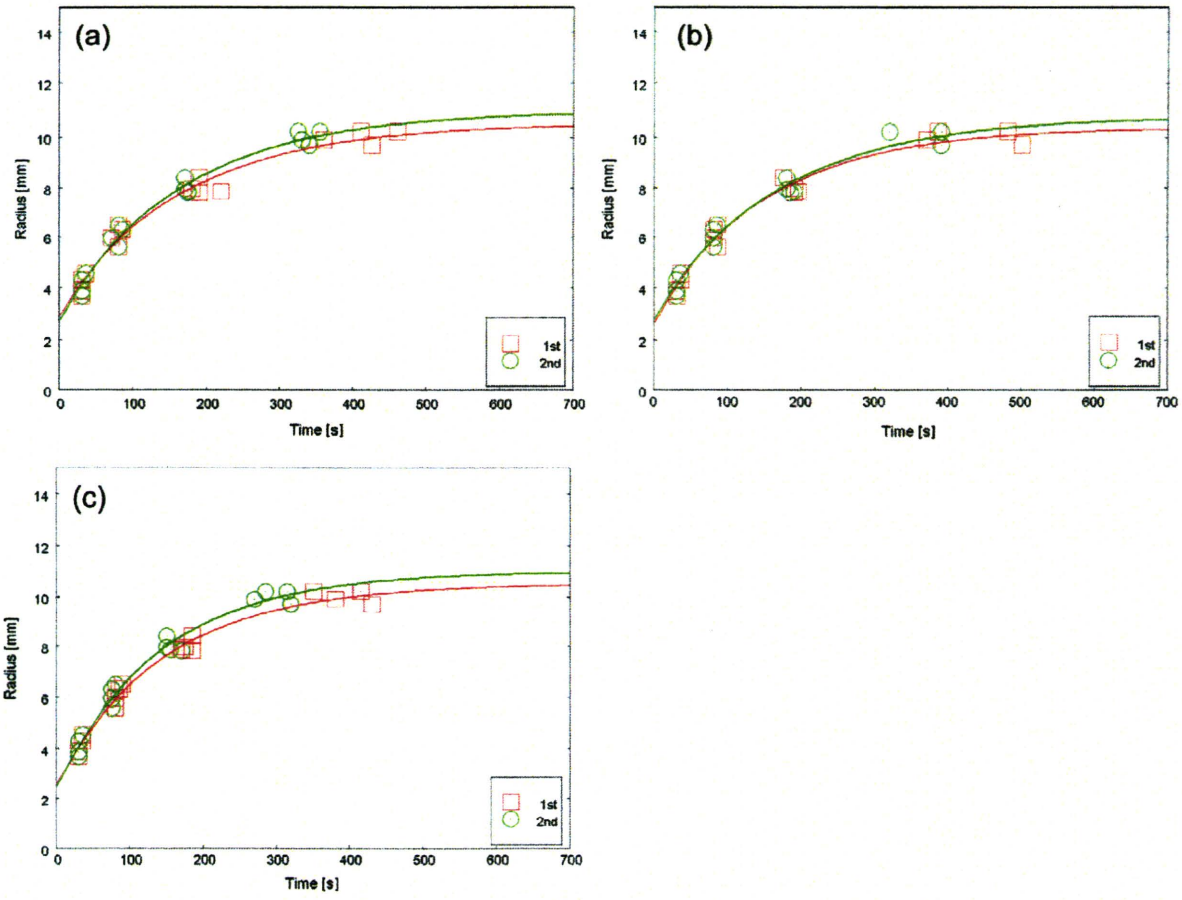

Fig. 10. Freezing functions in the experiments of liver.

Table 2
Parameters for freezing function in the experiments of liver obtained by the least-square method.

		a	$b \times 10^2$	c
Liver 1	1st	−7.61	−0.62	10.52
	2nd	−8.23	−0.62	10.97
Liver 2	1st	−7.70	−0.67	10.36
	2nd	−7.99	−0.62	10.77
Liver 3	1st	−7.95	−0.67	10.52
	2nd	−8.54	−0.70	11.02

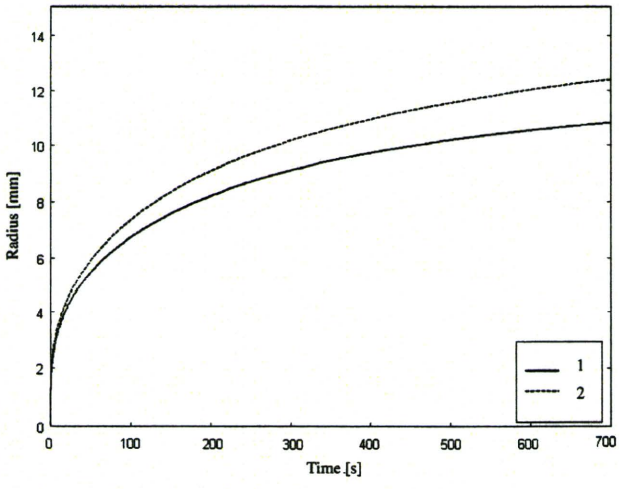

Fig. 11. Freezing curves by analytical solution.

Table 3
Parameters used for the calculation of analytical solution.

	1	2
R_p (mm)	1.15	1.15
S_m (W/m^3)	1200	1200
T_p (K)	−135.0	−135.0
T_0 (K)	37.0	37.0
T_i (K)	−2.0	−2.0
h_{sf} (J/kg)	334000	334000
ϖ_{eff} (/s)	0.02	0.02
k_i (W/m K) [5]	0.147	1.758
k_c (W/m K) [5]	0.0586	0.502
ρ_i (kg/m^3) [5]	100	1000
ρ_c (kg/m^3) [5]	100	1000
c_i (J/kg K) [5]	1675	1675
c_c (J/kg K) [5]	3349	3349
Cr	8.6	11.9
ω^*	0.15	0.18

more, we defined the freezing function by applying the least-square method to temperature data at each cycle, and analyzed the freeze-thaw sequence.

As a result of the analysis with the isothermal curve and the freezing function, the frozen area of the iceball was larger in the second cycle than in the first cycle. On the other hand, the frozen area in the third cycle was not significantly larger than in the second cycle. For the purpose of comparison, we also conducted the freeze-thaw cycle with the liver and the kidney as a non-aerated organ. In either organ, the frozen area in the second cycle was not larger than in the first cycle. From the viewpoint of thermal property, there is no dramatic change between the first cycle and

the second cycle in non-aerated organs, and the frozen area consequently is believed to make almost no change. In the meantime, it is believed that there was a significant change in thermal properties in the lung between the first cycle and the second cycle, yet there was no such significant change between the second cycle and the third cycle. As a significant change in thermal property, the bleeding at the first cycle conceivably infiltrates the lung. Basically, in the lung cryoablation, it is supposed that bleeding in the first freeze-thaw cycle increases the thermal diffusivity around the cryoprobe and it is enabled to freeze a greater area in the second freezing. Consequently, it is necessary to repeat the freeze-thaw cycle twice or more in the cryoablation of the lung cryoablation.

Acknowledgment

This work was supported by Grant-in-Aid for Scientific Research (21591823) of the Japanese Ministry of Education, Culture, Sports, Science and Technology.

References

[1] M. Kawamura, Y. Izumi, N. Tsukada, K. Asakura, H. Sugiura, H. Yashiro, K. Nakano, S. Nakatsuka, S. Kuribayashi, K. Kobayashi, Percutaneous cryoablation of small pulmonary malignant tumors under computed tomographic guidance with local anesthesia for nonsurgical candidates, J. Thorac. Cardiovasc. Surg. 131 (2006) 1007–1013.
[2] S. Nakatsuka, M. Kawamura, H. Sugiura, K. Nakano, Y. Izumi, K. Kobayashi, M. Jinzaki, S. Hashimoto, S. Kuribayashi, G. Wakabayashi, M. Kitajima, Preliminary experience with percutaneous cryoablation for malignant lung tumors under CT fluoroscopic guidance (in Japanese), Low Temp. Med. 30 (2004) 9–15.
[3] A.A. Gage, J. Baust, Mechanisms of tissue injury in cryosurgery, Cryobiology 37 (1998) 171–186.
[4] Y. Izumi, T. Oyama, E. Ikeda, M. Kawamura, K. Kobayashi, The acute effects of transthoracic cryoablation on normal lung evaluated in a porcine model, Ann. Thorac. Surg. 79 (2005) 318–322.
[5] C.Y. Lee, J. Bastacky, Comparative mathematical analyses of freezing in lung and solid tissue, Cryobiology 32 (1995) 299–305.
[6] J.C. Bischof, J. Bastacky, B. Rubinsky, An analytical study of cryosurgery in the lung, J. Biomech. Eng. 114 (1992) 467–472.
[7] S. Permpongkosol, T.L. Nicol, R.E. Link, I. Varkarakis, Q.J. Zhai, L.R. Kavoussi, S.B. Solomon, Differences in ablation size in porcine kidney, liver, and lung after cryoablation using the same ablation protocol, AJR Am. J. Roentgenol. 188 (2007) 1028–1032.
[8] M. Kawamura, Y. Izumi, N. Tsukada, S. Nakatsuka, H. Yashiro, M. Inoue, K. Iwata, T. Nagasawa, On freezing function of vital organ using cryoprobe as heat source, Low Temp. Med. 34 (2008) 23–28.
[9] A. Nakayama, Y. Kuwahara, K. Iwata, M. Kawamura, The limiting radius for freezing a tumor during percutaneous cryoablation, ASME Trans. J. Heat Transfer 130 (2008) 111101.
[10] T.E. Cooper, G.J. Trezek, Rate of lesion growth around spherical and cylindrical cryoprobes, Cryobiology 7 (1971) 183–190.
[11] B.S. Morse, T.S. Yoo, D.T. Chen, P. Rheingans, K.R. Subramanian, Interpolating implicit surfaces from scattered surface data using compactly supported radial basis functions, in: International Conference on Shape Modeling and Applications, 2001, pp. 89–98.
[12] M.L. Woolley, D.A. Schulsinger, D.B. Durand, I.S. Zeltser, W.C. Waltzer, Effect of freezing parameters (freeze cycle and thaw process) on tissue destruction following renal cryoablation, J. Endourol. 16 (2002) 519–522.
[13] J.K. Seifert, C.D. Gerharz, F. Mattes, F. Nassir, K. Fachinger, C. Beil, T. Junginger, A pig model of hepatic cryotherapy. In vivo temperature distribution during freezing and histopathological changes, Cryobiology 47 (2003) 214–226.
[14] T. Mala, B. Edwin, T. Tillung, Hol.P. Kristian, O. Søreide, I. Gladhaug, Percutaneous cryoablation of colorectal liver metastases: potentiated by two consecutive freeze-thaw cycles, Cryobiology 46 (2003) 99–102.
[15] A.V. Dilley, D.Y. Dy, A. Warlters, S. Copeland, A.E. Gillies, R.W. Morris, D.B. Gibb, T.A. Cook, D.L. Morris, Laboratory and animal model evaluation of the Cryotech LCS 2000 in hepatic cryotherapy, Cryobiology 30 (1993) 74–85.
[16] G.J. Stewart, A. Preketes, M. Horton, W.B. Ross, D.L. Morris, Hepatic cryotherapy: double-freeze cycles achieve greater hepatocellular injury in man, Cryobiology 32 (1995) 215–219.

ELSEVIER

European Journal of Cardio-thoracic Surgery xxx (2011) xxx–xxx

EUROPEAN JOURNAL OF CARDIO-THORACIC SURGERY

www.elsevier.com/locate/ejcts

Effect of cutting technique at the intersegmental plane during segmentectomy on expansion of the preserved segment: comparison between staplers and scissors in *ex vivo* pig lung

Keisuke Asakura, Yotaro Izumi *, Mitsutomo Kohno, Takashi Ohtsuka, Masayuki Okui, Kohei Hashimoto, Takashi Nakayama, Hiroaki Nomori

Division of General Thoracic Surgery, Department of Surgery, School of Medicine, Keio University, Tokyo, Japan

Received 7 December 2010; received in revised form 6 February 2011; accepted 10 February 2011

Abstract

Objective: Cutting the intersegmental plane by using a stapler during segmentectomy might interfere with the expansion of the preserved lung due to visceral pleura caught in a staple line, especially in a large regional segmentectomy, such as left upper division or basal segmentectomy. We compared the preserved lung volume after segmentectomy among the methods using stapler, sharp dissection, and their combination for cutting the intersegmental plane in *ex vivo* pig lungs. We also examined a covering effect of polyglycolic acid mesh and fibrin glue. **Methods:** To assume a large regional segmentectomy in clinical practice, segments of the left caudal lobe except the lateral segment 2 (L2 segment) were resected, and the lung volume of the preserved L2 segment was measured. The intersegmental plane was cut by the following three methods: (1) stapler ($n = 8$); (2) scissors ($n = 8$); and (3) the combined method, that is, cutting the shallow lung tissue with scissors and the deep one with stapler ($n = 8$). The opened intersegmental plane was covered with polyglycolic acid mesh and fibrin glue. The air leakage was checked by injecting air through the bronchus at pressures of up to 30 cmH_2O. Thereafter, normal saline was injected through the bronchus at pressures of 10, 20, and 30 cmH_2O, to measure lung volumes by the volume-displacement method. **Results:** Polyglycolic acid mesh and fibrin glue prevented air leakage completely at up to 30 cmH_2O. At the saline injection pressures of 10, 20, and 30 cmH_2O, the mean volumes of L2 segment were 72 ± 14, 96 ± 14, and 109 ± 26 ml with the stapler; 86 ± 11, 117 ± 19, and 135 ± 39 ml with scissors; and 98 ± 10, 140 ± 20, and 155 ± 40 ml with the combined methods, respectively. The volume of the preserved L2 segment was significantly lower with the stapler method than with either the scissors or combined method at each pressure ($p < 0.01$). The difference was not significant between the scissors and combined methods. **Conclusions:** Coverage with polyglycolic acid mesh and fibrin glue prevented air leakage from the opened intersegmental plane. The stapler interferes with the expansion of preserved lung in comparison to scissors or combined methods in a large regional segmentectomy.

Keywords: Lung cancer; Segmentectomy; Pulmonary function; Air leakage

1. Introduction

With an increasing number of patients with small-sized non-small-cell lung cancer, the importance of pulmonary segmentectomy has been growing. Some Japanese surgeons have reported the superiority of segmentectomy over lobectomy for preserving pulmonary function [1,2], but others refute this [3], of which difference may relate to the method used to cut the intersegmental plane during segmentectomy, that is, using a stapler versus an electric scalpel. The advantages of the former are its simplicity and less postoperative air leakage, but it may interfere with lung expansion due to the visceral pleura caught in the staple line. Therefore, to expand the preserved lung sufficiently, some surgeons cut the intersegmental plane by using an electric scalpel along the intersegmental plane, which is depicted between the inflated segment and deflated one [4–8]. We previously reported that a large regional segmentectomy, such as a left upper division segmentectomy, and the resection of more than three segments, such as a basal segmentectomy, could not preserve sufficient pulmonary function [2]. Therefore, the cutting procedure for intersegmental plane would be critical for preserving pulmonary function, especially in large regional segmentectomy. However, the technique using an electric scalpel might cause postoperative air leakage from the opened intersegmental plane. While the deflated–inflated line at the intersegmental plane is sharply defined at the shallow lung tissue, it sometimes becomes blurred at the deep tissue. In addition, to take a sufficient margin from the tumor, the lung

* Corresponding author. Address: Division of General Thoracic Surgery, Department of Surgery, School of Medicine, Keio University, 35 Shinanomachi, Shinjuku-ku, Tokyo 160-8582, Japan. Tel.: +81 3 5363 3806; fax: +81 3 5363 3499.
E-mail address: yotaroizumi@a2.keio.jp (Y. Izumi).

1010-7940/$ – see front matter © 2011 European Association for Cardio-Thoracic Surgery. Published by Elsevier B.V. All rights reserved.
doi:10.1016/j.ejcts.2011.02.021

DOCTOPIC: 10, 11, 14

should be frequently cut beyond the intersegmental plane, which also causes the air leakage. Therefore, even in the technique by using the electric scalpel, the stapler would be helpful for cutting deep intersegmental planes.

Therefore, the present experiment, using *ex vivo* pig lung, examined the following points: (1) whether or not the stapler method for cutting the whole lung tissue on intersegmental plane interferes with the expansion of preserved lung compared with that using scissors; and (2) whether or not the combined technique, that is, cutting the shallow lung tissue with scissors and the deep one with a stapler, interferes with the expansion of the preserved lung. To mimic a large regional segmentectomy in clinical practice, we removed all segments except the lateral segment 2 (L2 segment) from the left caudal lobe and measured the volume of the preserved L2 segment. In addition, to evaluate the usefulness of polyglycolic acid (PGA) mesh and fibrin glue for covering the intersegmental plane, pressure resistance test was also examined.

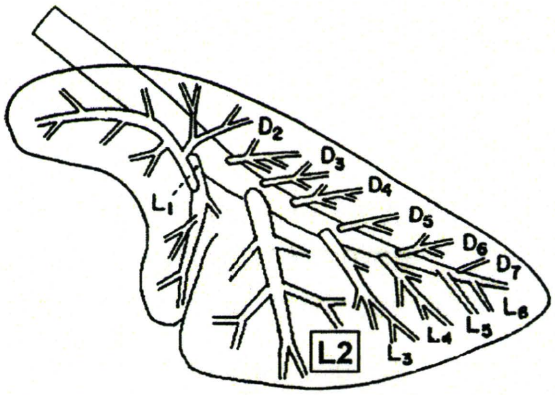

Fig. 1. Schematic lateral aspect of the pig left lung. The left caudal lobe consists of dorsal segments 2–7, medial segments 4 and 5, ventral segments 2–5, and the lateral segments 2–6. Dorsal and medial segments cannot be seen in the lateral aspect.

2. Materials and methods

2.1. Experimental protocol

The *ex vivo* left lungs obtained from slaughtered pigs, aged from 6 to 10 months and weighing approximately 100 kg, were used in the present study. The left lung consists of middle lobe and caudal lobe. Of these, the L2 segment is the largest segment (Fig. 1). To assume a large regional segmentectomy in clinical practice, all segments of the left caudal lobe except the L2 segment were resected, preserving the L2 segment. A flexible 12-Fr catheter was inserted into the L2 segmental bronchus, followed by ligation of the root of bronchus. Air was pumped into the catheter to create a border between the inflated L2 segment and deflated other lung tissue, as previously reported [4–7] (Fig. 2). The border between the inflated and deflated lung tissue was cut using the following three techniques: (1) stapler method (GIA: 6 cm in length and 4.8 mm in thickness; Covidien Co. USA) ($n = 8$); (2) scissors method ($n = 8$); and (3) combined method, that is, cutting more than half of the shallow border by scissors, followed by cutting the deep one by stapler ($n = 8$) (Fig. 3(A)–(C)). The intersegmental plane opened with scissors was covered with PGA mesh (Neoveil®, Kyoto Ika, Co., Kyoto, Japan) and fibrin glue (Bolheal®, The Chemo-Sero-Therapeutic Research Institute, Kumamoto, Japan), as reported previously (Fig. 3(D)) [9]. Briefly, a PGA mesh was used to completely cover the opened intersegmental plane, followed by coating with 1 ml each of fibrinogen and thrombin.

Prior to resection, the weight of the whole left lung and the L2 segment was measured to take into account the difference of lung size among the animals. The weight of the preserved L2 segment was measured after resection. Through the catheter inserted into the bronchus of L2 segment, air was injected to examine the air leakage before measuring lung volume. The air was injected consistently at the pressures of 10, 20, and 30 cmH_2O while dripping saline on the intersegmental plane to check for the absence of air bubbles. The absence of air leakage was mandatory for the accuracy of the following measurement of lung volume.

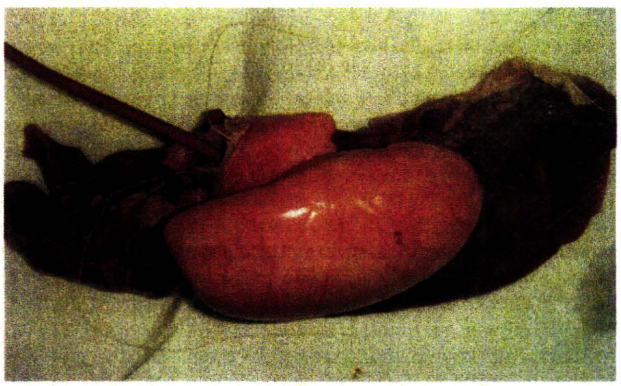

Fig. 2. L2 segment was inflated by selective inflation through the catheter inserted into the L2 segmental bronchus to delineate the deflated–inflated line.

Because the lung inflated with air could not be submerged in water for measurement of lung volume by the volume-displacement method [10], we injected normal saline into the segmental bronchus after checking air leakage. Normal saline was injected into L2 segmental bronchus at pressures of 10, 20, and 30 cmH_2O. The lung volume at each pressure was measured by the volume-displacement method. The volume/weight ratio of the L2 segment at each pressure was calculated as follows: volume of L2 segment with infusion of saline (ml)/weight of L2 segment before infusion of normal saline (g). Lung expansion around the intersegmental plane was also compared macroscopically among the three methods.

All animal studies were approved by the School of Medicine, Keio University Institutional Animal Care and Use Committee, and were carried out in accordance with the *Guide for the Care and Use of Laboratory Animals* published by the National Academies Press.

2.2. Statistical analysis

Data are expressed as means ± standard deviations. The data for each method were compared by the Mann–Whitney

Please cite this article in press as: Asakura K, et al. Effect of cutting technique at the intersegmental plane during segmentectomy on expansion of the preserved segment: comparison between staplers and scissors in *ex vivo* pig lung. Eur J Cardiothorac Surg (2011), doi:10.1016/j.ejcts.2011.02.021

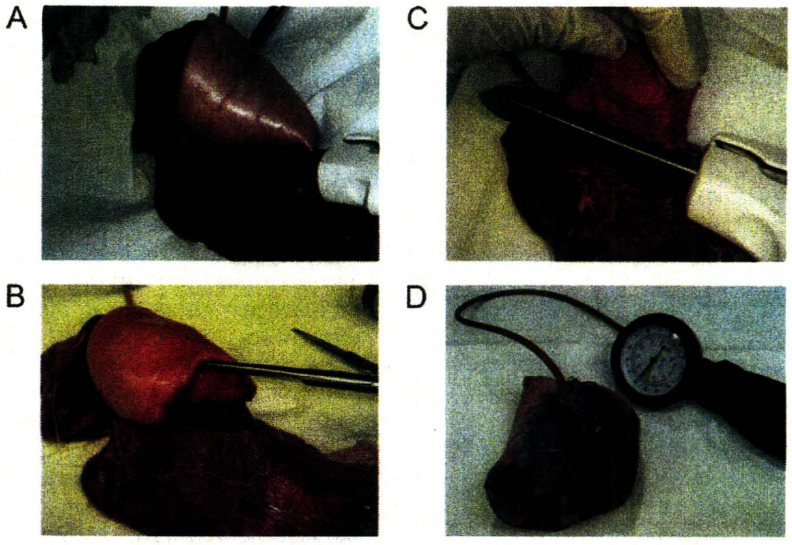

Fig. 3. (A) Stapler method, i.e. the border was cut by using a stapler ($n = 8$). (B) Scissors method, i.e. the border was completely cut by scissors ($n = 8$). (C) Combined method, i.e. more than half of shallow border was cut by scissors, followed by cutting the deeper one with a stapler ($n = 8$). (D) Covering the intersegmental plane with polyglycolic acid (PGA) mesh and fibrin glue to prevent air leakage. A manometer indicates that airway pressure is 30 cmH_2O.

U test (StatView; Abacus, Berkeley, CA, USA). The *p* value < 0.01 was considered statistically significant.

3. Results

In all three methods, air leakage from the intersegmental plane was never seen, at the pressure up to 30 cmH_2O.

There were no significant differences in the weights of the whole left lung and the L2 segment, or in the volume/weight ratio between the left lung and L2 segment among the methods (Table 1).

Figs. 4–6 show the volume/weight ratio of the L2 segment at the injected pressures of 10, 20, and 30 cmH_2O, respectively. At the pressure of 10 cmH_2O, the mean volumes of the L2 segment were 72 ± 14, 96 ± 14, and 109 ± 26 ml with the stapler, scissors, and combined methods, respectively. Those volume/weights were 2.8 ± 0.7, 3.9 ± 0.4, and 4.3 ± 0.4 ml g^{-1} for the stapler, scissors, and combined methods, respectively (Fig. 4). The mean volume/weight ratio with the stapling method was significantly lower than those with the scissors and combined ones ($p = 0.006$ and 0.0008, respectively). There was no significant difference in the volume/weight ratio between the scissors and combined methods.

At 20 cmH_2O, the mean volumes of the L2 segment were 86 ± 11, 117 ± 19, and 135 ± 39 ml with the stapler scissors, and combined methods, respectively. The volume/weight ratios were 3.3 ± 0.7, 4.8 ± 0.6, and 5.3 ± 0.5 ml g^{-1} for the

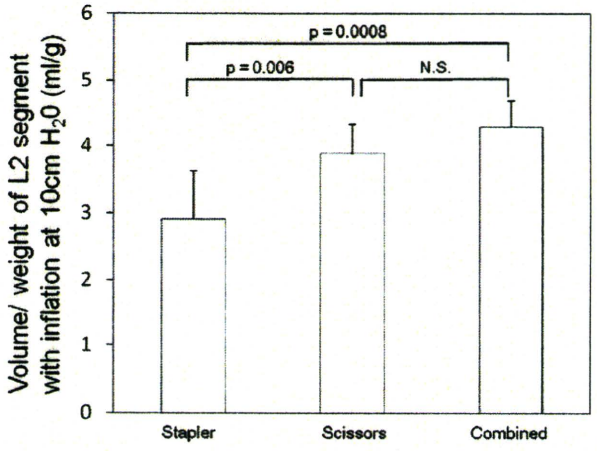

Fig. 4. Volume/weight of L2 segment with inflation at 10 cmH_2O ($n = 8$).

stapler, scissors, and combined methods, respectively (Fig. 5). The value with the stapler method was significantly lower than those with the scissors and combined ones ($p = 0.005$ and 0.0008, respectively). There were no significant differences in the volume/weight ratio between the scissors and combined methods.

At 30 cmH_2O, the mean volume of the L2 segment was 98 ± 10, 140 ± 20, and 155 ± 40 ml with the stapler, scissors, and combined methods, respectively. The volume/weight ratios were 3.8 ± 0.6, 5.7 ± 0.6, and 6.0 ± 0.6 ml g^{-1} for the

Table 1. Weight of the left whole lung and left L2 segment.

Weight of the lung	St ($n = 8$)	Sc ($n = 8$)	C ($n = 8$)	Difference
The left whole lung (g)	238 ± 18	243 ± 16	239 ± 33	N.S.
Left L2 (g)	26 ± 6	25 ± 2	26 ± 7	N.S.
Left L2/the left whole lung (%)	11 ± 2	10 ± 1	11 ± 1	N.S.

St, stapler method; Sc, scissors method; C, combined method; N.S.; not significant.

Please cite this article in press as: Asakura K, et al. Effect of cutting technique at the intersegmental plane during segmentectomy on expansion of the preserved segment: comparison between staplers and scissors in *ex vivo* pig lung. Eur J Cardiothorac Surg (2011), doi:10.1016/j.ejcts.2011.02.021

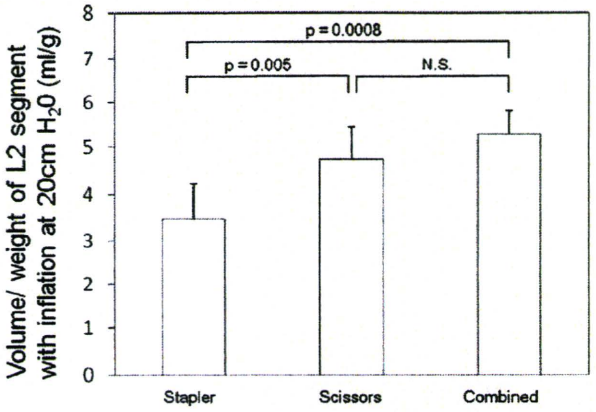

Fig. 5. Volume/weight of L2 segment with inflation at 20 cmH_2O (n = 8).

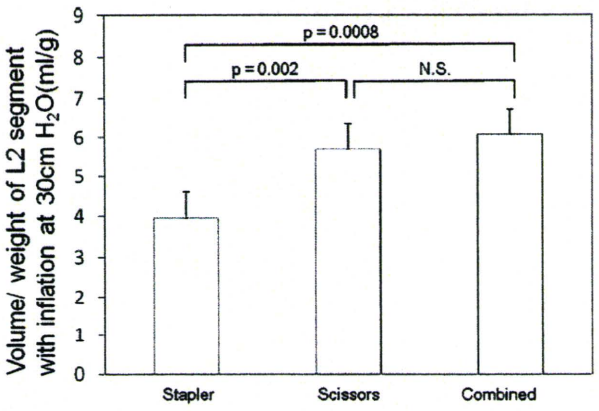

Fig. 6. Volume/weight of L2 segment with inflation at 30 cmH_2O (n = 8).

stapler, scissors, and combined methods (Fig. 6). The value with the stapler method was significantly lower than those with the scissors and combined ones (p = 0.002 and 0.0008, respectively). There was no significant difference in the volume/weight ratio between the scissors and combined methods.

Fig. 7 shows gross sections of L2 segment cut by the three methods. While the intersegmental plane was caught in the staple line on using the stapler, causing partial atelectasis, it was expanded well without any atelectasis by the scissors and combined methods.

4. Discussion

Three important points arise from this study: (1) the stapler method decreased the volume of the preserved segment significantly more than the scissors or combined method in the large regional segmentectomy; (2) there was no significant difference in the preserved volume between the scissors and combined methods; and (3) PGA mesh and fibrin glue successfully blocked air leakage from the opened intersegmental plane at up to 30 cmH_2O of airway pressure.

Decrease in the lung volume by the stapler method in comparison to the scissors or combined method should be due to the finding that the lung tissue including visceral pleura was caught in a staple line, causing partial atelectasis. Because the weights of L2 segment were not different among the three methods, the stapler method did cut the lung tissue accurately at the intersegmental plane similar to the other two methods. While the stapler method can cut the lung tissue simply, the interference for lung expansion would be a major weakness. The present study was carried out in *ex vivo* lungs, rather than in live pigs, so that accurate volume evaluation by the volume-displacement method was possible. However, because of this, long-term outcomes on the atelectasis around the staple line could not be followed up. While long-term follow up is necessary to address this issue, the results may be difficult to interpret due to postoperative changes, however.

When cutting the intersegmental plane along its deflated–inflated line, the line sometimes becomes blurred in the deep lung tissue in clinical practice. In addition, to take a sufficient surgical margin from a tumor, the cutting line often has to exceed over the intersegmental plane. These conditions often cause postoperative air leakage. The present experiment showed that using the stapler for the deep lung tissue not only secured the expansion of preserved lung but also would be effective for preventing air leakage.

In the present study, we assumed a large regional segmentectomy in clinical practice, such as left upper segmentectomy and basal segmentectomy. To reproduce a large regional segmentectomy in a pig lung, there is no choice except the present procedure, that is, preserving the L2

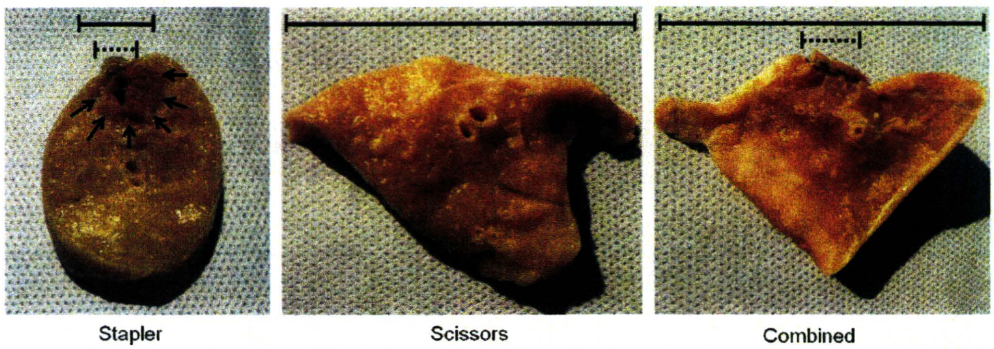

Fig. 7. Gross sections of L2 segment cut by a stapler, scissors, and combined methods. Solid line indicates the intersegmental planes cut by each method. Dotted line indicates the stapled planes of stapler or combined method. Arrows show the area of atelectasis in the stapler method.

Please cite this article in press as: Asakura K, et al. Effect of cutting technique at the intersegmental plane during segmentectomy on expansion of the preserved segment: comparison between staplers and scissors in *ex vivo* pig lung. Eur J Cardiothorac Surg (2011), doi:10.1016/j.ejcts.2011.02.021

segment, because the anatomy of the other segmental bronchus is complicated, which makes the other types of segmentectomy impossible. The L2 segment is the largest among these segments. Therefore, the preserved L2 segment is similar to a preserved small segment after large regional segmentectomy in clinical practice, such as lingular segment in left upper division segmentectomy and apical segment in the basal segmentectomy. Of course, it is possible that the differences between the stapler group and the scissors group may not have been as significant if the preserved segment had been larger.

In addition to the partial atelectasis at the staple line, the stapler method cannot preserve the intersegmental vein, which has a role of venous flow of nearly half of the preserved segment. The block of venous flow along the intersegmental plane by stapler therefore causes an impairment of gas exchange leading to decrease in pulmonary function. By contrast, the scissors or combined method can preserve the intersegmental pulmonary vein, enabling preservation of gas exchange of the preserved segment.

It has been reported that the covering the opened intersegmental plane with PGA mesh and fibrin glue is useful for preventing postoperative air leakage [9]. PGA mesh is a soft and thin (0.15 mm in thickness) absorbable material, which, together with fibrin glue, makes it possible to block air leakage from the peripheral lung tissue without significant interference with lung expansion because of the excellent elasticity of both materials. In the present experiment, covering the opened intersegmental plane with these materials could prevent the air leakage even at the pressure of 30 cmH_2O, which would be useful in clinical practice.

We conclude that a stapler for cutting intersegmental plane interferes with the expansion of the preserved lung comparing with the scissors or combined methods in large regional segmentectomy. However, a stapler for cutting the deep intersegmental plane not only does not interfere with the lung expansion but also would be useful for preventing air leakage. Coverage with PGA mesh and fibrin glue can prevent air leakage from the opened intersegmental plane.

References

[1] Harada H, Okada M, Sakamoto T, Matsuoka H, Tsubota N. Functional advantage after radical segmentectomy versus lobectomy for lung cancer. Ann Thorac Surg 2005;80:2041–5.

[2] Yoshimoto K, Nomori H, Mori T, Kobayashi H, Ohba Y, Shibata H, Tashiro K, Shiraishi S, Kobayashi T. Quantification of the impact of segmentectomy on pulmonary function by perfusion single-photon-emission computed tomography and multidetector computed tomography. J Thorac Cardiovasc Surg 2009;137:1200–5.

[3] Ginsberg RJ, Rubinstein LV. Randomized trial of lobectomy versus limited resection for T1 N0 non-small cell lung cancer. Lung Cancer Study Group. Ann Thorac Surg 1995;60:615–22 [discussion 622–613].

[4] Tsubota N, Ayabe K, Doi O, Mori T, Namikawa S, Taki T, Watanabe Y. Ongoing prospective study of segmentectomy for small lung tumors. Study group of extended segmentectomy for small lung tumor. Ann Thorac Surg 1998;66:1787–90.

[5] Okada M, Koike T, Higashiyama M, Yamato Y, Kodama K, Tsubota N. Radical sublobar resection for small-sized non-small cell lung cancer: a multicenter study. J Thorac Cardiovasc Surg 2006;132:769–75.

[6] Nomori H, Ikeda K, Mori T, Kobayashi H, Iwatani K, Kawanaka K, Shiraishi S, Kobayashi T. Sentinel node navigation segmentectomy for clinical stage IA non-small cell lung cancer. J Thorac Cardiovasc Surg 2007;133:780–5.

[7] Tsubota N. An improved method for distinguishing the intersegmental plane of the lung. Surg Today 2000;30:963–4.

[8] Atkins BZ, Harpole Jr DH, Mangum JH, Toloza EM, D'Amico TA, Burfeind Jr WR. Pulmonary segmentectomy by thoracotomy or thoracoscopy: reduced hospital length of stay with a minimally-invasive approach. Ann Thorac Surg 2007;84:1107–12 [discussion 1112–1103].

[9] Matsumura Y, Okada Y, Shimada K, Endo C, Chida M, Sakurada A, Sato M, Kondo T. New surgical technique of pulmonary segmentectomy by ultrasonic scalpel and absorbable sealing materials. Kyobu Geka 2004;57:31–7.

[10] Scherle W. A simple method for volumetry of organs in quantitative stereology. Mikroskopie 1970;26:57–60.

Please cite this article in press as: Asakura K, et al. Effect of cutting technique at the intersegmental plane during segmentectomy on expansion of the preserved segment: comparison between staplers and scissors in *ex vivo* pig lung. Eur J Cardiothorac Surg (2011), doi:10.1016/j.ejcts.2011.02.021